Impact of macromolecular crowding on the mesomorphic behavior of lipid self-assemblies

Agustín Mangiarotti, Luis A. Bagatolli

PII: S0005-2736(21)00176-0

DOI: https://doi.org/10.1016/j.bbamem.2021.183728

Reference: BBAMEM 183728

To appear in: *BBA - Biomembranes*

Received date: 29 March 2021

Revised date: 19 July 2021

Accepted date: 6 August 2021

Please cite this article as: A. Mangiarotti and L.A. Bagatolli, Impact of macromolecular crowding on the mesomorphic behavior of lipid self-assemblies, *BBA - Biomembranes* (2018), https://doi.org/10.1016/j.bbamem.2021.183728

Impact of macromolecular crowding on the mesomorphic behavior of lipid self-assemblies

Agustín Mangiarotti[a] and Luis A. Bagatolli[a,b,*]

[a]Instituto de Investigación Médica Mercedes y Martín Ferreyra - INIMEC (CONICET) - Universidad Nacional de Córdoba, Friuli 2434, 5016, Córdoba, Argentina.
[b]Departamento de Química Biológica Ranwel Caputto, Facultad de Ciencias Químicas, Universidad Nacional de Córdoba, Córdoba, Argentina.

*Correspondence to lbagatolli@immf.uncor.edu

Abstract

Using LAURDAN fluorescence we observed that water dynamics measured at the interface of DOPC bilayers can be differentially regulated by the presence of crowded suspensions of different proteins (HSA, IgG, Gelatin) and PEG, under conditions where the polymers are not in direct molecular contact with the lipid interface. Specifically, we found that the decrease in water dipolar relaxation at the membrane interface correlates with an increased fraction of randomly oriented (or random coil) configurations in the polymers, as Gelatin>PEG>IgG>HSA. By using the same experimental strategy, we also demonstrated that structural transitions from globular to extended conformations in proteins can induce transitions between lamellar and non-lamellar phases in mixtures of DOPC and monoolein. Independent experiments using Raman spectroscopy showed that aqueous suspensions of polymers exhibiting high proportions of randomly oriented conformations display increased fractions of tetracoordinated water, a configuration that is dominant in ice. This indicates a greater capacity of this type of structure for polarizing water and consequently reducing its chemical activity. This effect is in line with one of the tenets of the Association Induction Hypothesis, which predicts a long-range dynamic structuring of water molecules via their interactions with proteins (or other polymers) showing extended conformations. Overall, our results suggest a crucial role of water in promoting couplings between structural changes in macromolecules and supramolecular arrangements of lipids. This mechanism may be of relevance to cell structure/function when the crowded nature of the intracellular milieu is considered.

Keywords: Lipid polymorphism, macromolecular crowding, LAURDAN fluorescence, protein secondary structure, lipid membrane hydration, PEG.

1. Introduction

The intracellular milieu of virtually all cellular systems is characterized by very high concentrations of macromolecules, estimated to be around 200-350 mg/mL[1,2]. In this extremely crowded environment, the distance between macromolecules is estimated to be around 1-2 nm, enough to accommodate just a few water molecules in these interstices[3]. As a consequence, it can be expected that the physical properties of intracellular water will be affected by this environment and will be considerably different from those of the bulk[3]. This challenges the idea that the intracellular milieu can be described as a regular aqueous solution of ions and proteins, as it is generally assumed in the dominant model describing the cell[3–7].

Although there is still a consensus that the lipid component of biological membranes acts as a barrier, and is described as a (mostly static) bilayer entity compartmentalizing “solution like” environments in the cell, there is currently a re-emergence of colloidal concepts to describe the spatial organization of the intracellular milieu. In particular, it has been recently shown that the cell interior can be dynamically compartmentalized without the assistance of lipid membranes through the emergence of 3D liquid phase transitions, with a crucial participation of polyelectrolytes such as intrinsically disordered proteins[8–10]. This observation poses an interesting challenge regarding the barrier role attributed to lipids and, more importantly, raises interesting questions about the way lipid self-assemblies are integrated into these biological coacervates.

The colloidal properties of the cell stem crucially from the state of cellular water (the major component of all living systems) and, in this respect, there is a sound, still unrefuted, theory of colloids available to describe this type of phenomenon, called the Association Induction Hypothesis (AIH). Among others, the AIH incorporates an original treatment of water as part and parcel of a crowded, dynamic protein-water-ion/solute system[11–14]. Briefly, it develops a treatment of the energetics of water association to the repetitive peptide bonds in *extended protein conformations (*called *extroverted* systems*)*, which offer properly-spaced alternating dipoles that orient and polarize water in successive layers. This structure of successive layers of polarized-oriented water dipoles is cooperatively modulated by metabolic activity (via cardinal adsorbents such as

ATP)[13,14]. The polarization of water causes a reduction in their translational as well as rotational motional freedom and, more importantly, influences its chemical activity[13,14]. This has been substantiated by a large amount of experimental work performed both *in vitro* and *in vivo*[11–14].

In a series of studies published over the last six years we have tested and validated several core tenets of the AIH[15–19] using a system consisting of dense suspensions of living *Saccharomyces cerevisiae* cells displaying a central metabolism characterized by glycolytic oscillations. Among other things, we established that the extent of water dipolar relaxation in the cell interior is coupled to, and oscillates synchronously with, the concentration of metabolites (such as ATP and NADH). Importantly, oscillations, glycolytic and all others, are abolished when the polymerization of actin is compromised, suggesting that the actin cytoskeleton is an active component of the process that gives rise to the metabolic oscillations and all those that are coupled to them[15,18]. Interestingly, and very relevant for this article, we also observed that the cytosolic oscillations in water dipolar relaxation can be coupled to those existing in membranous structures[15,16,20]. This led us to hypothesize that metabolic changes may regulate mesomorphic changes in lipid self-assemblies via the physical state of cell water[20]. This last hypothesis represents an original contribution from our group to the framework of the AIH, which barely addresses the role of lipids. Therefore, this paper attempts to test *in vitro,* with different spectroscopic methods, whether structural features of proteins (and another polymer like PEG) may influence the physical properties of lipid self-assemblies via changes in the dynamical and collective structural properties of water.

2. Materials and Methods

2.1. Materials

The lipids 1,2-dipalmitoyl-sn-glycero-3-phosphocholine (DPPC), 1,2-dilauroyl-sn-glycero-3-phosphocholine (DLPC), 1,2-dioleoyl-sn-glycero-3-phosphocholine (DOPC), 1-oleoyl-rac-glycerol (GMO) and cholesterol, were purchased from Avanti Polar Lipids (USA). 6-lauroyl-2-dimethylaminonaphthalene (LAURDAN) was from Invitrogen (Denmark). 1,4-Bis(4-methyl-5-phenyl-2-oxazolyl)benzene (DMPOPOP), Polyethylene glycol (PEG) of average molecular weights of 400

and 20000, Gelatin, Guanidine hydrochloride (GdnHCl), Phosphate Saline Buffer (PBS) and cellulose dialysis membranes (cut-off ~14kDa) were purchased from Sigma (Argentina). High purity Human Serum Albumin and Immunoglobulin G were gifts from the Laboratorio de Hemoderivados (University of Córdoba, Córdoba, Argentina). Organic solvents were purchased from Sintorgan S.A. (Argentina). All solvents and chemicals were of the highest commercially available purity. Deionized water (18 MΩ cm) was obtained from an Osmoion purifier (Apema, Argentina).

2.2. Methods

Lipid dispersions and dialysis experiments

All lipid stock solutions were prepared in Cl_3CH:CH_3OH 2:1 v/v. To prepare the different lipid aqueous dispersions, desired aliquots of the lipid organic solutions were dried in a clean vial under a stream of nitrogen and then placed under vacuum for 1 hour. The samples were then hydrated in PBS (0.01 M phosphate buffer, 0.0027 M potassium chloride and 0.137 M sodium chloride, pH 7.4) to a final concentration of 0.5 mg/mL during 1 hour at temperatures above the melting transition of the pure lipid or desired mixture. During this procedure the samples were subjected to two cycles of vortexing (30 seconds each). Multilamellar vesicles (MLVs) composed exclusively of phospholipids were used for fluorescence measurements right after preparation, while dispersions (cubic or lamellar phases) containing GMO were allowed to equilibrate overnight and vortexed prior to data collection. All lipid samples were labelled with LAURDAN (0.5% mol) by premixing the probe with the lipids in organic solutions. LAURDAN stock solution was prepared in chloroform at a final concentration of 1 mM.

The setup and procedures for the dialysis experiments are described in detail in the supporting material (Section A). Briefly, the lipid dispersion was placed in a dialysis sac and placed in a tube containing the desired polymer/protein aqueous suspension (Figure S1), letting it equilibrate overnight. After this procedure the lipid dispersion was removed from the dialysis sac to immediately proceed with the fluorescence measurements. All proteins used in these experiments were first dialyzed against deionized water and then lyophilized

before use. The protein/PEG colloidal suspensions, at a desired concentration, were prepared in the same buffer used to disperse the lipids (PBS).

2.2.a. Spectroscopic measurements

Raman Spectroscopy

Raman measurements were performed using a Horiba Lab Raman confocal microscope (LABRAM-HR 800) equipped with a 4x objective for liquids. Protein/polymer solutions were placed into 3 mL quartz cuvettes. The spectra were taken between 2800 and 4000 cm^{-1} using a 600 lines.mm^{-1} grating and 10 s acquisition time with 10 accumulations per second. The excitation wavelength used was 633 nm (He−Ne laser, 1.5 cm^{-1} spectral resolution) at 5 mW laser power. Protein/polymer solutions at 0.1% w/v concentration were used, since higher concentrations led to Rayleigh scattering hindering the Raman signal. All measurements were performed at room temperature and the spectra were measured in at least three different zones of each sample. Previously to the measurements, calibrations were done with a silicon pattern. Data analysis was performed using OriginLab.

Attenuated total reflectance Fourier Transform Infrared (ATR-FTIR) Spectroscopy

ATR-FTIR spectra of proteins were recorded on a Nexus FT-IR spectrophotometer (Nicolet) equipped with a single reflection diamond accessory (Golden Gate, Specac). The measurement chamber was purged with nitrogen to reduce water vapor distortions in the spectra. Samples were spread on the diamond crystal, flushed with nitrogen and rehydrated using nitrogen saturated in deuterium to obtain the protein spectra. A total of 256 accumulations were recorded at 20 °C using a nominal resolution of 2 cm^{-1}. After subtraction of water vapor and side chain contributions, the baseline of spectra were corrected and the area was normalized between 1600 and 1700 cm^{-1}. All data were processed and analysed using Kinetics software (SFMB, Brussels, Belgium). For details on spectral analysis see supporting information (section D, Figure S5).

Fluorescence measurements

Fluorescence measurements were performed in an ISS Chronos FD fluorometer (Champaign, IL, USA) upgraded with a Xenon arc lamp and an excitation monochromator. For fluorescence emission spectra and Generalized Polarization measurements, the lamp was set at 360 nm excitation wavelength, with the polarizer in vertical position and a KV408 filter in the emission path. This setup filters out scattering effects including those related to Wood's anomaly[21]. Each lipid dispersion was always prepared in duplicate with and without the fluorescent probe in order to test for potential contributions of scatter or fluorescent contaminants.

For lifetime measurements, phase and modulation data were obtained using a 374 nm diode for excitation with the emission collected either through a 470±20 nm bandpass filter or a 500 nm long pass filter (see below lifetime phasor section). A KV370 filter was placed in the excitation path to filter out undesired contributions of the excitation diode. Data were collected until the standard deviation from each measurement of phase delay (ϕ) and modulation (M) were at most 0.2° and 0.004, respectively. Diode modulation frequency was ranged logarithmically from below to above the crossover of ϕ and modulation M in at least 15 steps (between 10 MHz and 150 MHz), and analysed for each sample using the Vinci 3 software (ISS) assuming decays containing either 1 or 2 discrete components. χ^2 scores were all below 1 (see supporting information, section H, table S1). In order to eliminate polarization effects[22], the excitation and emission polarizers were set at magic angles (0°-55° respectively). A solution of DMPOPOP in ethanol was used as reference with a fluorescence lifetime of 1.45 ns[23]. All fluorescence measurements were carried out by triplicate at 20.0 ± 0.1°C. The data reported correspond to the mean value of the measurements.

2.2.b. Fluorescence Analysis

LAURDAN Generalized Polarization (GP_{ex}) function and GP_{ex} spectra

The fluorescence emission spectrum of LAURDAN is sensitive to the extent of water dipolar relaxation process occurring at the local probe milieu. Specifically, dipolar relaxation caused by the rotational modes of water molecules occurring during the fluorescence lifetime of the probe affects the energy of the excited

state, causing a red shift in the fluorescence emission. This mechanism has been extensively discussed and reviewed for LAURDAN in lipid membranes (see e.g. [24–26]). Briefly, it has been shown that the relaxation effect exerted by water molecules located at the membrane interface is particularly pronounced for bilayers exhibiting liquid-disordered (L_α) phases (the probe emits from a relaxed state), but negligible for those exhibiting solid-ordered (gel or L_β) phases (the probe emits from an unrelaxed state). The emission spectra for these two cases are shown in Figure 1a. Notice the red shifted, broader, LAURDAN emission spectrum observed in the L_α phase respect to that observed in the L_β phase (DOPC and DPPC respectively in Figure 1a). When there is coexistence of both phases in the bilayer, LAURDAN emission comes from both, relaxed and unrelaxed states, and in consequence a broader emission spectrum can be observed (e.g. the equimolar mixture of DPPC and DOPC in Figure 1a). This spectral behavior can be quantified using the GP_{ex} function as:

$$GP_{ex} = \frac{I_B - I_R}{I_B + I_R} \qquad (1)$$

where I_B and I_R correspond to the intensities at the blue and red edges of the emission spectrum (respectively) using a given excitation wavelength[24,25]. In this work, I_B and I_R correspond to 440 and 490nm respectively. The LAURDAN GP_{ex} function has been extensively utilized to obtain information about lateral packing of lipid bilayers[26]. In this respect a strong correlation between the LAURDAN GP_{ex} function and the order parameter obtained by NMR in lipid bilayers has been recently confirmed[27]. In general, high LAURDAN GP_{ex} values (0.5-0.6) have been reported for bilayers in the L_β phase state, whereas low LAURDAN GP_{ex} values (below 0) where reported for L_α phase. In addition, intermediate GP_{ex} values have been observed when phase segregation is present and in the case of bilayers exhibiting liquid-ordered phases induced by cholesterol[28,29].

While discrete GP_{ex} values at a given wavelength can be useful for comparative measurements, GP_{ex} information can be further exploited by constructing a GP_{ex} spectrum. This analysis, originally described by Parasassi and collaborators[24,26], allows to visually determine from the slope of the GP

spectrum, if relaxed (slope<0), unrelaxed states (slope=0) or a mixture of both states (slope>0), are present in a given sample. A GP_{ex} spectrum can be constructed by changing the excitation wavelength while measuring GP_{ex} at each point, as exemplified in Figure 1b for membranes displaying L_α, L_β and their coexistence.

Phasor plots

LAURDAN spectral and lifetime data can be further analysed using phasor plots. This analysis offers a powerful, model free, graphic method to characterize spectral[30] and lifetime information[31]. Briefly, the analysis consists in the calculation of a vector (G,S) i.e. the phasor, in which coordinates correspond to the real and imaginary part of a Fourier transform computed using spectral or lifetime data as described below.

LAURDAN spectral phasors

The LAURDAN spectrum is transformed using the following expressions for x and y coordinates:

$$y = G_{(\lambda)} = \frac{\sum_\lambda F(\lambda)\cos(\frac{2\pi n(\lambda-\lambda_0)}{L})}{\sum_\lambda F(\lambda)} \qquad (2)$$

$$x = S_{(\lambda)} = \frac{\sum_\lambda F(\lambda)\sin(\frac{2\pi n(\lambda-\lambda_0)}{L})}{\sum_\lambda F(\lambda)} \qquad (3)$$

where $F(\lambda)$ are the fluorescence intensity values, λ_0 is the initial wavelength of the spectrum, L is the length of the spectrum and n is the harmonic value. In general, L=180 (from 420 to 600 nm) and n=1 were used for phasor calculations, unless otherwise specified. The angular position of the phasor in the plot is related to the center of mass, while the radial position depends on the full width at half maximum (FWHM) of the spectrum[32]. This is well exemplified in Figure 1c, where the phasor plot for the fluorescence spectra depicted in Figure 1a are shown. As observed, when moving from DPPC (L_β) to DOPC (L_α), the phasor for LAURDAN moves counter clockwise due to the red shift of the center of mass, and closer to the radial center (0;0) due to the increase in the

FWHM. When the mixture DPPC:DOPC is plotted, the corresponding phasor falls in the linear trajectory between the pure components[32]. This is due to the vectorial properties of the Fourier space: if the phasors for the pure components are known, then the mixtures will fall in between as the linear combination of these two reference states since L_α/L_β coexistence, i.e. relaxed and unrelaxed states, occur in this particular lipid mixture[32,33] because the coexistence of the two phases. In general, variations in the position on this trajectory can be also expected if the extent of water relaxation at the membrane interface is modified by other means. One interesting example is that of the phasor calculated for DLPC at 20°C. First, it can be seen that the DLPC phasor is also located on the trajectory between DPPC and DOPC, suggesting that this trajectory is a general feature for L_α to L_β phase transition. However, the DLPC phasor position does not coincide with that for pure DOPC at 20°C, even though these two bilayers exist in the L_α phase (Figure 1c). DLPC is a saturated lipid that forms bilayers and has a main phase transition temperature (T_m) of -2°C, different to that of the unsaturated DOPC, which is -17°C. This chemical difference impacts the stability of the interactions established among lipids (k_BT), causing slight variations in packing and consequently water dipolar relaxation processes at the interface. Specifically, at 20°C, the position of DLPC in the phasor plot is closer to the end point defined by DPPC on the DOPC-DPPC trajectory, indicating that the extent of dipolar relaxation is lower than for DOPC at the same temperature. However, when DLPC is heated to 35°C its phasor is displaced on the L_β-L_α trajectory to a point near DOPC at 20°C, as shown in Figure 1c indicating that both interfaces bear a similar extent of dipolar relaxation. The case of DLPC is a good example showing how a membrane existing in the same phase state (L_α) and keeping the same composition can experience changes in water dynamics by tuning an external parameter (temperature in this case). It is important to remark that this effect is particularly noticeable when the membranes are in the L_α phase, since the L_β phase has much slower dipolar relaxation dynamics than the LAURDAN fluorescence lifetime[26].

Taking into account this information it is reasonable to conclude that the trajectory L_β-L_α observed for lamellar configurations can be generalized for

lipids displaying this particular type of transition and, more important, whatever variation occurring in the phasor position on this trajectory will provide sensible information on variations in the hydration dynamics of the membrane. This analysis is used in our experiments when membranes are exposed to polymeric solutions (see results section, e.g. Figure 2). Overall, LAURDAN spectral phasors provide a powerful graphic way to evaluate changes in membrane hydration dynamics, without the need to assume a model, as is the case of the GP_{ex} function[32].

LAURDAN lifetime phasors

From lifetime measurements performed in the frequency domain, modulation (M) and phase (ϕ) data are obtained. This data can be transformed into the phasor coordinates by the following expressions:

$$y = G_{(\tau)} = Mcos(\phi) \quad (4)$$

$$x = S_{(\tau)} = Msin(\phi) \quad (5)$$

For a single-exponential decay, this vector describes a semicircle of radius 0.5 with a center at (0.5, 0) due to the relationship $M=cos(\phi)$[31]. Therefore, a fluorophore characterized by a single lifetime will always give rise to a phasor point that falls on this semicircle, typically referred to as the universal circle (see Figure 1D). The phasor points for fluorophores that present multiexponential decays are constrained within the universal circle, as described by Eqs. (4) and (5). Longer lifetimes will fall towards the origin (0;0), while shorter lifetimes will fall towards (1;0). Finally, in the presence of excited state reactions, as in the case of dipolar solvent relaxation or FRET, phasor data points can fall outside the universal circle[34,35].

Given the photophysics of LAURDAN, it has been suggested that it is possible to identify the presence of dipolar relaxation processes by using appropriate filters[36]. Specifically, using a 500 nm long pass filter (“red” filter) dipolar relaxation effects can be discriminated. This is exemplified in Figure 1d for DOPC (L_α) and DPPC (L_β) bilayers, where the blue filter shows the increment in lifetime associated to changes in polarity and relaxation, and the red filter shows

the marked decrease in dipolar relaxation when going from the L_α to the L_β phase state.

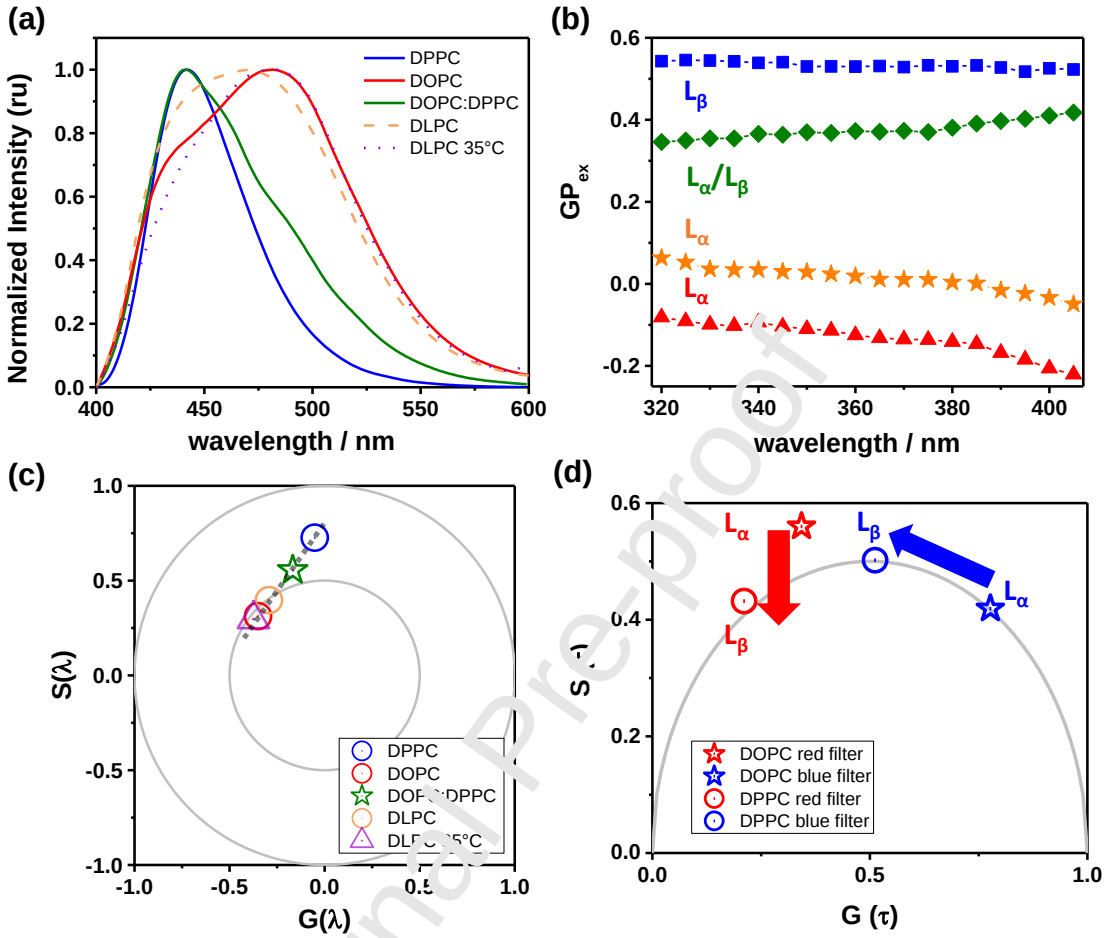

Figure 1. Examples of the different fluorescence parameters measured in our work. **(a)** Normalized LAURDAN fluorescence spectra at 20°C observed in DOPC, DLPC, DPPC, DPPC:DOPC 1:1 mol mixture, and DLPC membranes at 35°C. **(b)** LAURDAN GP_{ex} spectra for DOPC (red), DLPC (orange), DPPC:DOPC 1:1 mol mixture (green) and DPPC (blue). From the sign of the GP_{ex} spectrum slope the phase state of the membrane can be inferred. **(c)** Spectral phasor plot for the spectra shown in (a). The trajectory L_α-L_β is highlighted with the dashed line. **(d)** Lifetime phasor plot for LAURDAN observed in DOPC (L_α phase,★) and DPPC (L_β phase,⊙) obtained through the blue and red filters at 26 and 47 MHz, respectively (these frequencies were chosen arbitrarily for clarity, but the same effect is observed at all frequencies) The data obtained with the blue filter show a rise in the LAURDAN fluorescence lifetime as the membrane phase state changes from L_α to L_β phase. This is interpreted as decrease in membrane polarity and relaxation. The data obtained with the red filter show a decrease in dipolar relaxation as the membrane phase state changes from L_α to L_β phase.

3. Results

3.1. Effect of PEG crowding on the hydration of DOPC membranes

PEG is a compound commonly used as a molecular crowder due to its simple structure and inertness. The effect of PEG on lipids was extensively studied during the '80s and the beginning of the '90s. For example, phospholipid monolayers at the air-water interface show a condensation effect when PEG is

incorporated in the water phase, displaying changes in the monolayer surface potential. These effects were attributed to changes in the hydration of the lipid polar groups induced by PEG[37]. In addition, when PEG was added to liposome suspensions, it was shown that the polymer excludes from the vesicle surface[38] and dehydrates the membrane due to long range water structuration[39]. This was proven to be an indirect effect, since the same results were obtained either for aqueous PEG/liposome mixtures or PEG suspensions separated from the liposomes using a dialysis membrane[40].

In order to evaluate the effect of PEG on the hydration properties of lipid membranes, DOPC MLVs labelled with LAURDAN were prepared in presence of different concentrations of PEG 400 and their emission spectra were measured as shown in Figure 2a. DOPC was chosen for its low T_m, and in consequence its high extent of water dipolar relaxation at room temperature, allowing to better determine subtle changes in this parameter (see supporting information, Figures S2 and S3). It can be observed that with increasing PEG concentration the band at 440 nm is augmented, suggesting a less relaxed polar environment around the probe [24,26]. This effect becomes clearer when LAURDAN emission spectra are used to compute spectral phasors, as shown in Figure 2b. When PEG concentration is increased, the phasors gradually move along the L_α-L_β trajectory towards the L_β reference point, suggesting decreased dynamics of the interfacial water. This effect can be also connected with a stiffer lipid packing, consistent with results recently reported for DMPC small unilamellar vesicles[41].

Another quantitative way of evaluating the spectral changes observed in Figure 2a is by using the LAURDAN GP_{ex} function. Figure 2c shows the relative changes in GP_{ex} ($\Delta GP_{ex}=GP_{DOPC+PEG}-GP_{DOPC}$) when different concentrations of PEG are added to DOPC vesicles. It can be seen that the LAURDAN ΔGP_{ex} value becomes more positive when a small amount of PEG is included in the system reaching a maximum value at PEG concentrations of 30%. Assessment of the LAURDAN GP_{ex} spectra indicates that the L_α phase state persists at all PEG concentrations, but with a lower extent of relaxation as the GP_{ex} values increase with increasing PEG concentration (see Figure S4). Finally, when evaluating LAURDAN lifetimes, it can be seen that when using the blue filter there is an increase in LAURDAN fluorescence lifetime upon PEG addition, as

expected for a decrease in polarity and hydration dynamics (Figure 2d). In line with the information provided by the GP_{ex} spectra, the lifetime data obtained with the red filter suggest that dipolar relaxation persists in the sample upon PEG addition. From all these data it can be concluded that LAURDAN is responsive to crowding effects induced by PEG, supporting previous conclusions about membrane dehydration caused by the polymer due to long range water structuration[37–41].

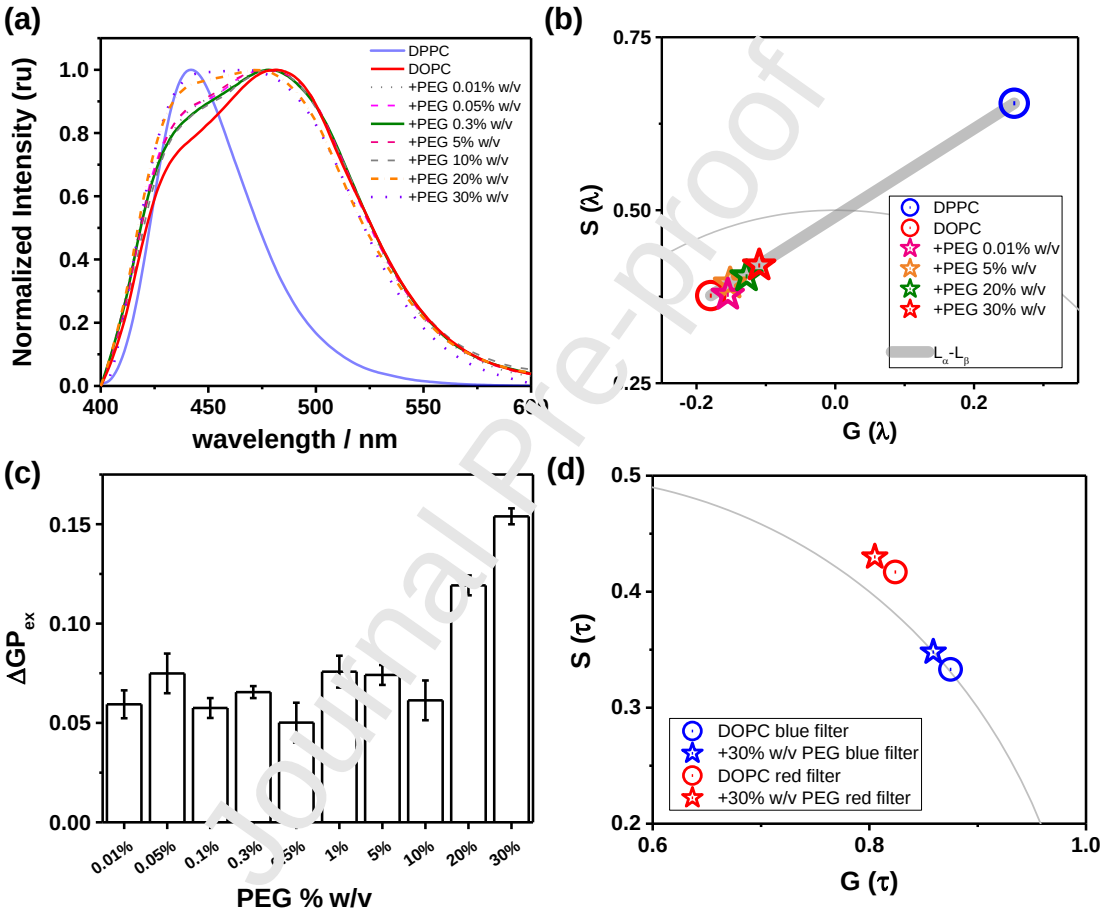

Figure 2. (a) Normalized LAURDAN fluorescence spectra at 20°C of DPPC, DOPC, and DOPC+PEG 400 at the compositions indicated. **(b)** LAURDAN spectral phasor plot of the spectra shown in (a). For clarity, only some compositions are shown. **(c)** LAURDAN ΔGP_{ex} for DOPC+PEG 400 at different concentrations. **(d)** Comparative lifetime phasor plot for LAURDAN in DOPC and DOPC+ PEG 30% w/v, obtained using the red and blue filters at 18 MHz.

3.2. Protein secondary structure modulates membrane hydration

According to AIH[12,13] proteins existing in extended configurations (for example, in random coil structures) can interact with water, largely reducing its rotational motional freedom affecting its chemical activity. This effect is much smaller in proteins in globular conformations, dominated by α-helix and β-sheet

secondary structures, which mostly favour intramolecular electronic interactions. In the language of the AIH these two situations (i.e. extended and globular proteins) are respectively called extroverted and introverted systems. With the aim of evaluating the effect of different proteins on membrane hydration, DOPC vesicles were incubated with protein suspensions under crowded conditions. HSA and IgG, two globular proteins differing in their secondary structure types and content, were selected as introvert models, and Gelatin, a protein with a large percentage of random coil in its structure, due to the great number of prolines and hydroxyprolines in its sequence[42], was selected as an extended (extrovert) model. The relative contributions of the distinct secondary structure elements for these three proteins were obtained from analysis of FTIR-ATR spectra and are summarized in Table 1. For HSA the alpha-helix structure is predominant, whereas in IgG beta-sheets and turns are the main secondary structural motifs, in line with previous reports[43–45]. For Gelatin, there is a prevalence of random coil structure[46–48]. Interactions of HSA and IgG with lipid membranes are well described in the literature[49–51] showing binding, and formation of aggregates[50]. Since we are particularly interested in discarding direct interactions between these two components, a dialysis membrane was used to separate the lipid dispersions from the proteins (see section 2.2.1 and supporting information, Figure S1).

Table 1. Percentage of secondary structure analysis from FTIR-ATR spectra*.

	Alpha-helix	Beta-sheet	Turns	Random coil
HSA	87.79	11.05	1.16	0
IgG	0	65.75	34.25	0
Gelatin	0	7.22	0	92.78

*for details see S5.

Figure 4 shows the effects of incubating DOPC membranes with a 5% w/v (50 mg mL^{-1}) solution of the proteins and PEG 20000 for comparison (higher MW PEG was used to avoid permeation trough the dialysis sac). This percentage was chosen to mimic crowding conditions (notice that diluted concentrations presented no changes in membrane hydration as seen in Figure S6 from the supporting information, while higher concentrations led to gelation of Gelatin).

The fluorescence emission spectra of LAURDAN labelled DOPC membranes show a gradual increase in the intensity of the 440 nm band in the order Gelatin>PEG>IgG>HSA, as depicted in Figure 3a. When the emission spectra are analysed using the spectral phasor method (Figure 3b) it can be seen that all points fall within the L_α-L_β trajectory, with a displacement towards the L_β position in the order Gelatin>PEG>IgG>HSA. Similarly, the relative change in the LAURDAN GP_{ex} and the LAURDAN fluorescence lifetime values increased following the same trend in the polymer series (see Figures 3 c,d and S6). All these results suggest that the polymers promote a decrease in the extent of water dipolar relaxation at the membrane interface, being more noticeable for Gelatin. It is important to mention that the results obtained with PEG 20000 (and also with the proteins) using the dialysis sac, are comparable to the results obtained in the previous section where the vesicles where prepared directly in aqueous suspensions of PEG400. This result is in line with a previous report on the indirect effect of PEG and its exclusion from membranes[40].

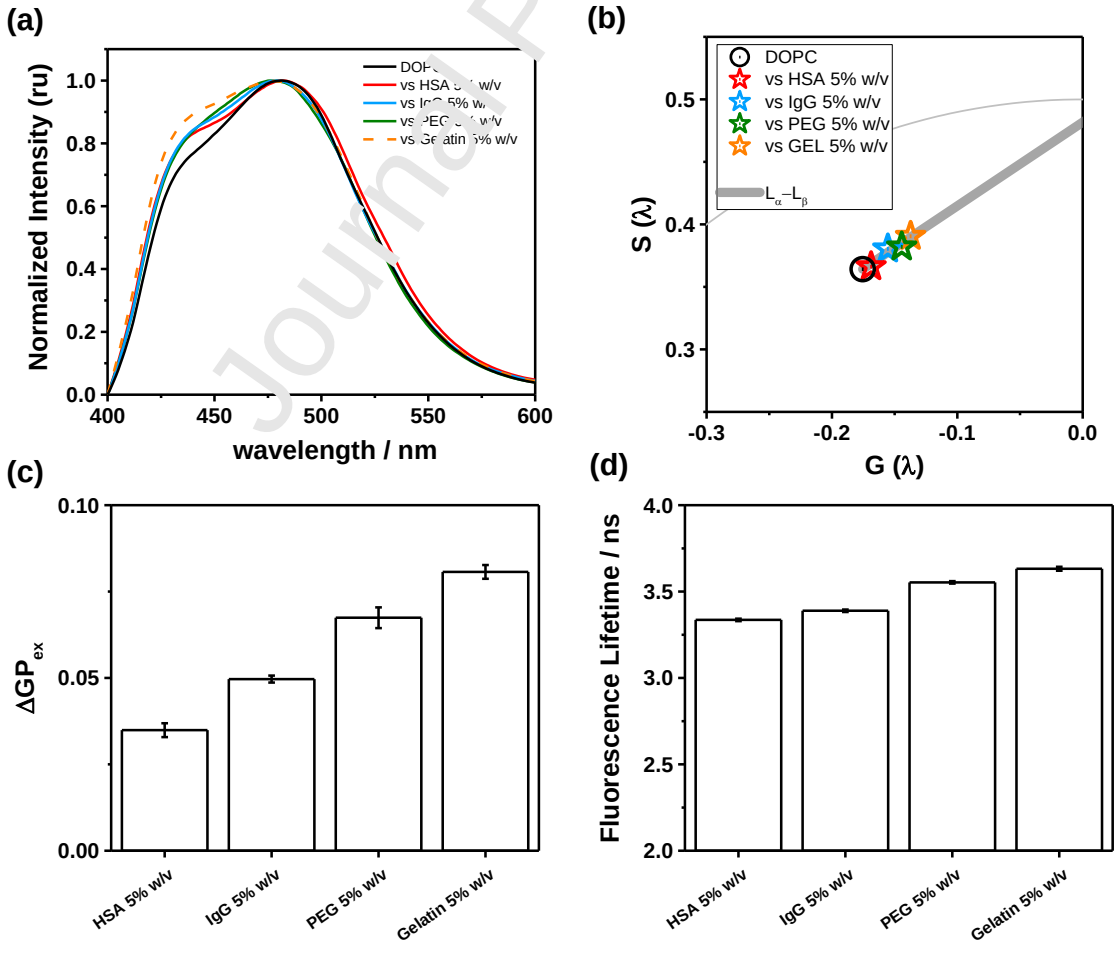

Figure 3. (a) Normalized fluorescence spectra at 20°C of LAURDAN in DOPC vesicles, and DOPC vs a solution of 5% w/v of the indicated protein/polymer. **(b)** Spectral phasor plot of the spectra shown in (a). **(c)** ΔGP_{ex} for DOPC vs the different proteins/polymer. **(d)** LAURDAN lifetime values obtained with the blue filter. These values were obtained by fitting one discrete exponential to phase and modulation data measured between 10-150 MHz.

Since there is a clear dependence of membrane dehydration on the differential contribution of the protein secondary structure, we decided to investigate how HSA, IgG and Gelatin impact the structure of water. For this purpose, we performed Raman spectroscopy measurements in aqueous suspensions of the proteins. The water band in the Raman spectrum is centred between 3000-3800 cm^{-1}, which is separated from the protein contribution that is located between 400-1700 cm^{-1}. The Raman spectra of water can be deconvolved into five sub-bands assigned to OH vibrations engaged in hydrogen-bonding and free vibrations[52]. The two main contributions are located at 3225 cm^{-1} and 3432, cm^{-1}, corresponding to tetracoordinated and dicoordinated water molecules, respectively[52]. In liquid water the 3432 cm^{-1} band is predominant, but when water freezes, the 3225 cm^{-1} becomes dominant, causing a spectral shift to lower wavenumbers [53]. When measuring the water band for solutions of proteins and PEG it can be observed that the contribution of the band corresponding to tetracoordinated water increases, indicating that the collective structure of water is changed in the presence of polymers. In the case of proteins this effect is notably higher when random coil structures are present, even at this low concentration, as observed for Gelatin. These results were analysed adapting the expression of the GP function described in equation (1), where I_B and I_R now correspond to the 3225 and 3432 cm^{-1} bands respectively. The values of this function, called $GP_{tetra/di}$, obtained for the different proteins and PEG is shown in Figure 4b.

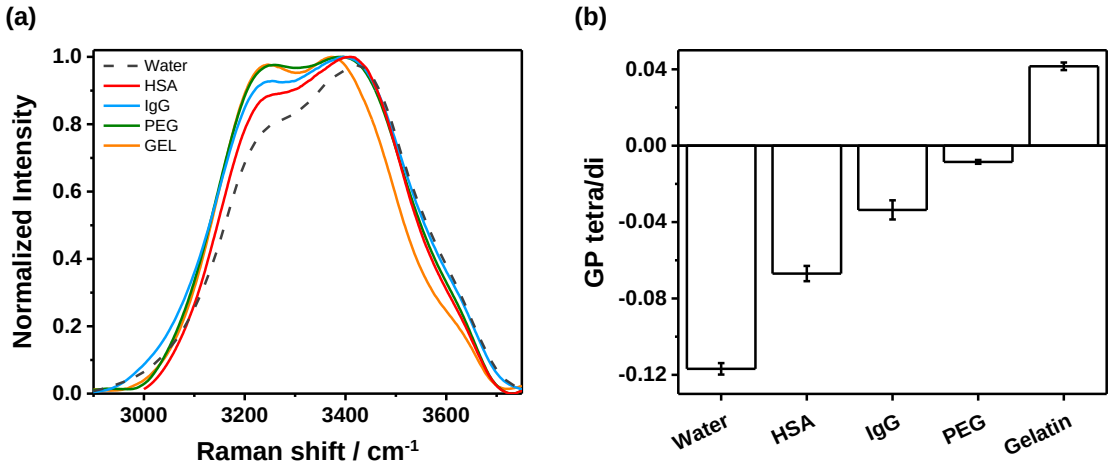

Figure 4. (a) Normalized Raman spectra of deionized water, and protein/PEG solutions at 0.1% w/v. The spectra correspond to the mean of at least three spectra taken at different zones of the sample. **(b)** Spectral changes are quantified with the GP function calculated for the intensity contributions of the bands at 3225 and 3432 cm^{-1} ($GP_{tetra/di}$), corresponding respectively to tetracoordinated and dicoordinated water molecules engaged in hydrogen bonds.

Interestingly, the structuration of water caused by these polymers follows the order Gelatin>PEG>IgG>HSA, mirroring the order observed in the experiments involving LAURDAN labelled membranes (Figure 3). This suggests that the impact that proteins/polymer exert on water structure couple to the dynamics of water existing at the membrane interface. The fact that PEG and Gelatin generate a major change in water long-range structuration is in agreement with the Polarized Oriented Multilayer Theory, a subsidiary theory of the AIH, proposed by Ling and collaborators[13,14,54,55], as will be discussed in the next section.

In order to further test whether protein secondary structure determines the extent of water long-range structuration, and consequently the changes in water dynamics at the membrane interface, we decided to explore the effects caused by structural changes in the same protein, i.e., a transition from globular to a fully extended configuration. This structural change can be caused by protein denaturation, destabilizing the protein tertiary structure and secondary motifs, producing a more disordered (extroverted) structure. For that purpose, vesicle dispersions were put in contact with solutions of the three proteins in native and denatured states using a dialysis sac. While no effects were observed for LAURDAN labelled DOPC membranes in contact with the native proteins at low concentration (0.5% w/v, Figure 5a), the same concentration of proteins

denatured in 6M GdnHCl led to marked effects on the LAURDAN labelled DOPC membrane emission spectra (Figure 5b), spectral phasors (Figure 5c) and relative changes in the LAURDAN GP_{ex} function (GP_{ex}, Figure 5d). These effects involve respectively an increase in the intensity of the 440 nm band, a displacement towards the L_β position within the L_α-L_β phasor trajectory and an increase in the relative change of the LAURDAN GP_{ex}. In addition, the shape observed for LAURDAN GP_{ex} spectra resemble in all cases that observed for membranes existing in the L_α phase state (Figure S7) but with higher GP_{ex} values when proteins are denatured, suggesting a decrease in the extent of water relaxation in the membrane.

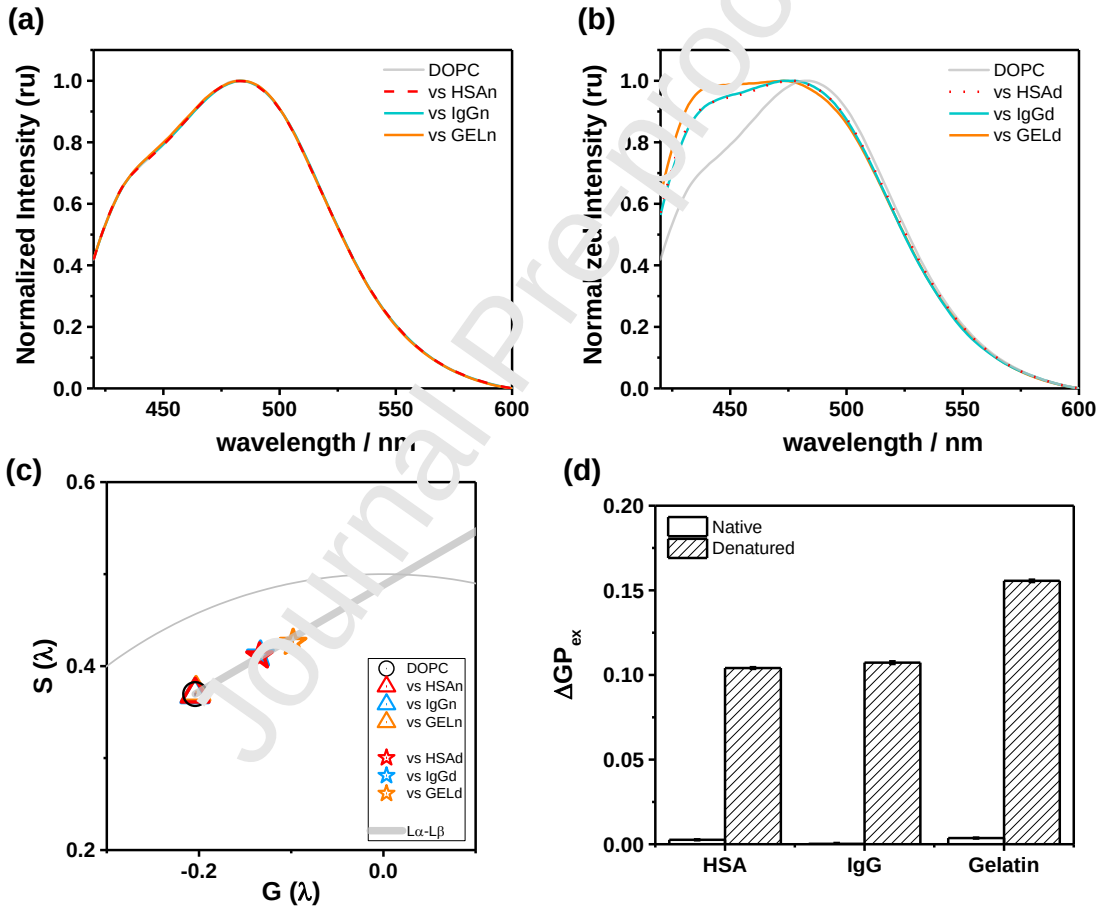

Figure 5. (a) Normalized fluorescence spectra of LAURDAN in DOPC vesicles in buffer and in the presence of 0.5% w/v of the different native (n) proteins. **(b)** Normalized fluorescence spectra of LAURDAN in DOPC vesicles in buffer and in the presence of 0.5% w/v of the different denatured (d) proteins **(c)** Spectral phasors of the spectra shown in (a) and (b). **(d)** LAURDAN ΔGP_{ex} for DOPC vesicles in contact with native and denatured protein solutions.

3.3. Changes in protein secondary structure can induce mesomorphic transitions in aqueous dispersion of lipids

Having found that protein secondary structure can differentially modulate the hydration properties of membranes via structuration of water, and consequently changes in its chemical activity, we asked whether membranes can experience mesomorphic transitions under similar circumstances. For these experiments we selected monoolein (GMO), a very well characterized lipid that exhibits a rich lyotropic mesomorphism[56–58] that has been studied for many decades for its advantages in protein crystallization, drug delivery, and food industry applications[58–60]. It is very well documented that pure GMO in excess water forms a Pn3m (double-diamond) cubic phases at 20°C[56–58], while when mixed with DOPC, it can transition from cubic Pn3m to lamellar L_α phase depending on composition[61,62].

The fluorescence spectrum of LAURDAN incorporated in pure GMO water dispersions is shown in Figure 6a. When compared to DOPC, it can be seen that for GMO the maximum of the spectrum is red shifted, near 497 nm, indicating that the probe is located in a more relaxed environment compared with DOPC bilayers. This is probably due to the higher degree of curvature exhibited by cubic phases when compared to bilayers [58,63–65]. The position for GMO in the spectral phasor diagram is displaced counter clockwise compared to DOPC bilayers (Figure 6b), as expected from the observed red shift. In line with this result the GP_{ex} value for GMO is -0.37, much lower than for that reported for L_α phases (see Figure 6c and GP_{ex} spectra in the supporting material, Figure S8). Regarding the fluorescence lifetime data obtained using the blue filter, GMO phase delay and modulation can be accurately adjusted with two discrete components of 3.08 ns and 1.1 ns with a χ^2 of 0.217 (Figure 6d and SI9). All these LAURDAN parameters that characterize the Pn3m cubic phase composed of pure GMO are clearly distinct to those observed for DOPC bilayers.

Figure 6 also shows the spectral and lifetime changes for mixtures of GMO with DOPC at different molar compositions. As mentioned above, the use of this mixture allows us to study the Pn3m-L_α transition[61,62]. When adding DOPC to GMO the LAURDAN spectra begin to appear blue shifted, with a progressive increase in the band at 440 nm. Figure 6b show that the LAURDAN spectral phasors for this mixture show a completely different trajectory compared to the L_α-L_β shown in the previous sections, defining a fingerprint for the Pn3m-L_α

transition. In addition, the GP_{ex} increases considerably with the addition of DOPC, as shown in Figure 6c, suggesting a gradual decrease in the extent of water dipolar relaxation in the system.

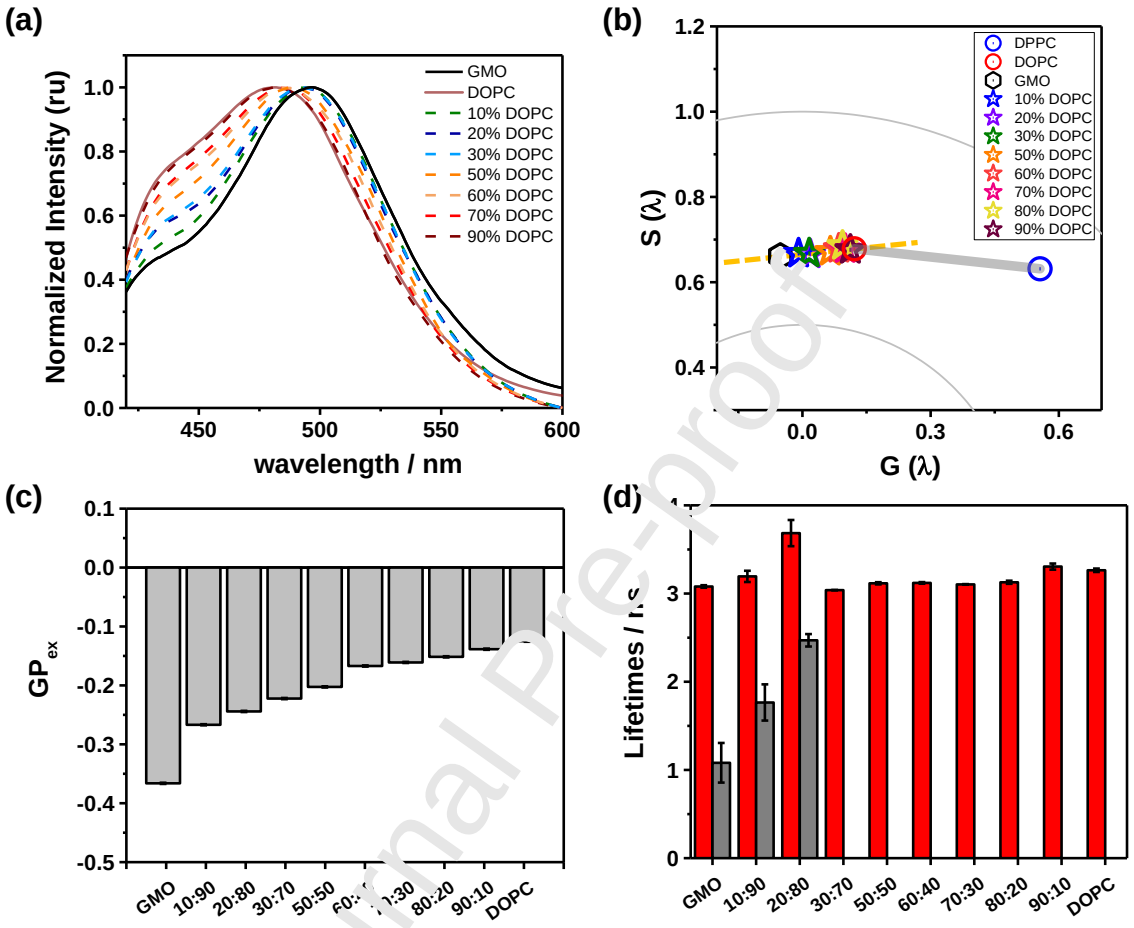

Figure 6. (a) Normalized fluorescence spectra of LAURDAN in pure DOPC and GMO dispersions, and in the indicated mixtures (mol:mol). **(b)** LAURDAN spectral phasors for the spectra shown in (a). The phasor for DPPC was included to depict the L_α-L_β transition (grey line). The Pn3m-L_α transition is indicated with the orange dashed line. Notice that the phasors are located at different coordinates compared to previous sections because a different range was used (from 420 to 700 nm, L=280). **(c)** Absolute GP_{ex} values for pure GMO and DOPC and their mixtures (the compositions indicated correspond to molar mixtures of DOPC:GMO). **(d)** LAURDAN lifetime values obtained using the blue filter. GMO, and DOPC:GMO 10:90 mol and 20:80 mol are well described by two discrete lifetimes, while all the other mixtures and pure DOPC were adjusted with a single exponential. For details on the fitting see S9.

Interestingly, fluorescence lifetimes can be adjusted with two discrete exponentials up to the composition DOPC:GMO 20:80 mol. However, when the percentage of DOPC is ≥30% the fluorescence lifetime is better described by a single exponential similar to that observed for pure DOPC (Figure 6d, Table

S1). These results are consistent with the prevalence of a Pn3m cubic phase up to 25% of DOPC and a presence of a L_α phase at higher proportions of DOPC (≥26%), as reported by Cherezov et al. using X-ray diffraction[61]. Thus, in order to select a point where the lyotropic transition Pn3m→L_α is completed, an upper limit at 30% of DOPC was arbitrarily selected.

With this information in mind we chose the DOPC:GMO 10:90 mol mixture (cubic phase) to evaluate the ability of PEG and denatured proteins to promote a lyotropic Pn3m→L_α transition. Figure 7a shows the spectral changes obtained with increasing PEG concentration. From the emission spectra it is noticeable how the fluorescence intensity of 440 nm band increases, with a concomitant blue shift at higher proportions of PEG. This is clearly visible in the spectral phasor plot shown in Figure 7b: with 5% w/v PEG the phasor is located in a position similar to that observed for DOPC:GMO 50:50 mol (Figure 6b), far beyond the point where the transition Pn3m-L_α occurs (DOPC:GMO 70:30 mol; marked in Figure 7b and 7d with a solid pink diamond). For higher PEG concentrations the phasor position surpasses the Pn3m-L_α transition point and moves towards the position of pure DOPC. At 30% w/v PEG the phasor falls in the L_α-L_β trajectory between DOPC and DPPC. This result clearly shows that PEG can induce a mesomorphic transition in the system via water long range structuration, implying changes in water activity.

It is interesting to highlight that when PEG is added to a pure GMO dispersion, the transition to L_α is observed for 30% w/v PEG (supporting information, Figure S10). For lower percentages it can be seen that there is a deviation from the Pn3m-L_α trajectory. When mixing GMO with DOPC the system can only transition from a cubic to a lamellar phase[61,62] and dehydration follows the Pn3m-L_α trajectory, as shown in Figure 7. However, pure GMO can undergo a Pn3m-Ia3d and a Ia3d-L_α transition[56–58] (see supporting information, Figure S10c). Moreover, it is possible to fall in regions of phase coexistence, or even in regions where the formation of a L_3 (sponge) phase[56–58,66,67] may occur. The case of pure GMO is clearly a more complex scenario, and therefore deviations for the Pn3m-L_α trajectory can occur as shown in Figure S10b from the supporting information.

Finally, Figures 7c and d show that denatured proteins can also induce a lyotropic transition in this system: for the three proteins the phasors are

localized beyond the DOPC:GMO 70:30 mol transition limit, more prominently in the case of denatured Gelatin.

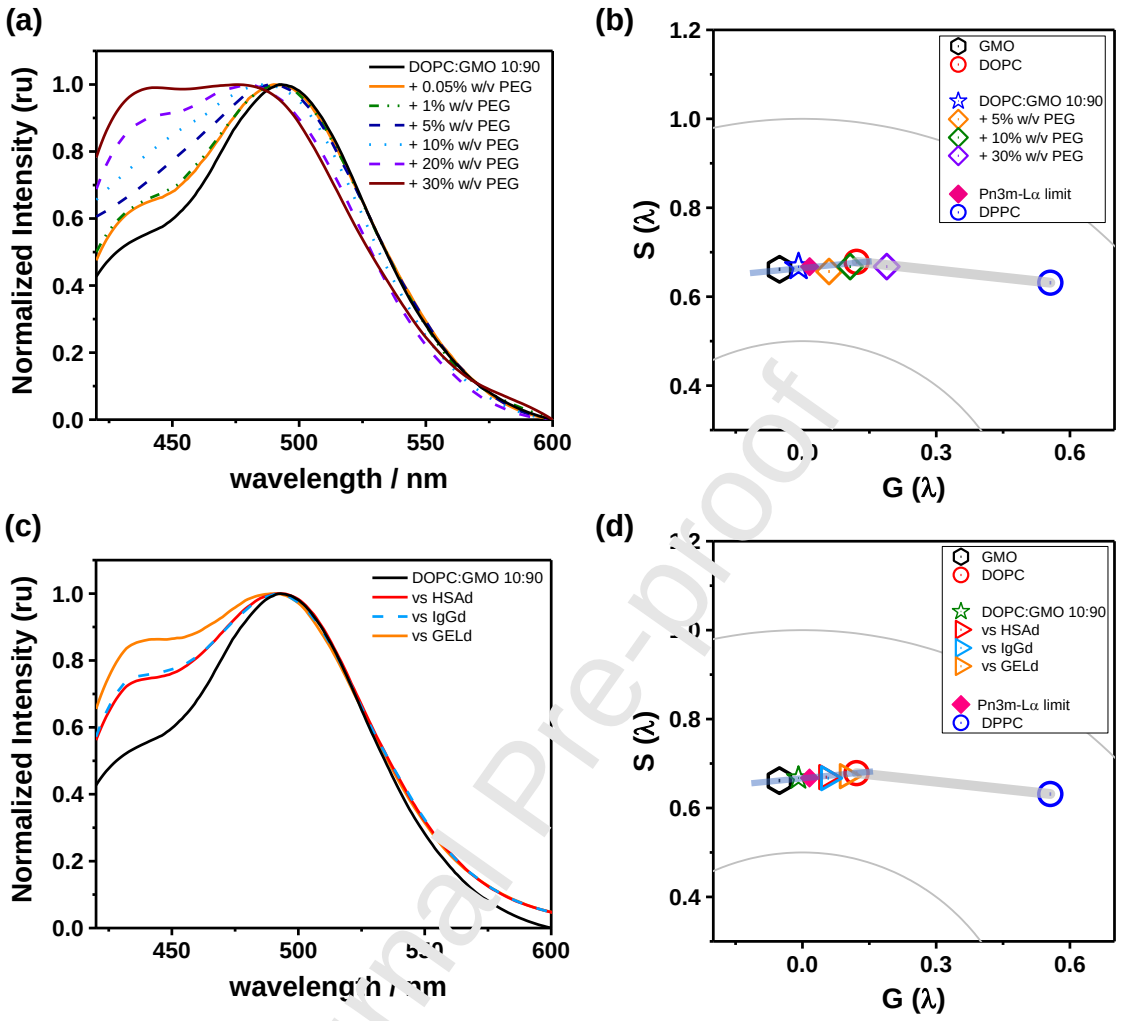

Figure 7. Normalized LAURDAN fluorescence spectra in DOPC:GMO 10:90 mol mixture dispersions with different concentrations of PEG 400 **(a),** or solutions of 0.5% w/v of the denatured proteins **(c)**. **(b, d)** Spectral phasors for the spectra shown in (a) and (c) respectively. The LAURDAN phasor obtained for DPPC was included as a reference. The Pn3m-L_α transition point is marked with a pink diamond.

4. Discussion

This paper attempts to test at *in vitro* conditions if particular structural features of proteins can influence the physical properties of lipid membranes through changes in the physicochemical properties of water. For this purpose, we exploited the exquisite sensitivity of LAURDAN fluorescence, which provides information on lipid packing and the hydration state of lipid membranes[26]. In this respect, we used a series of analytical tools, including spectral phasors[30,32], GP_{ex} and GP_{ex} spectra[24–26] and lifetime phasors[31,34,35]

(Figure 1), that allowed us to identify different states of the systems. Among them, we want to remark the use of the spectral phasor plots[32], which allows to define trajectories connecting different structural states of membranes. This analysis permits to visually monitor perturbations in the extent of water dipolar relaxation at the membrane interface mediated by the presence of polymers (Figures 2b, 3b, 5c, 6b and 7b). This methodology represents a very powerful analytical tool that has been previously exploited to evaluate changes in the composition of lipid mixtures[32] and comparatively monitor the hydration state of natural membranes in living cells using artificial membrane systems as a reference[68].

To perform part of our experiments we used a similar experimental design as the one utilized by Ling and collaborators to study the effect of different polymers (PEG, proteins) on their capacity to structure water, consequently affecting ionic activity, solute solvency, and osmotic behavior[69–71]. Specifically, the experimental setup consisted in a dialysis bag containing a crowded aqueous polymer suspension that is in contact with an aqueous medium containing the compounds of interest. This particular setup prevents direct interactions between the two parts of the system, with water being the only link between compartments. The main conclusion of Ling's experiments using this setup was that, in harmony with the Polarized Multilayer Theory of cell water[13], aqueous solutions of proteins (and polymers) bearing extended conformations (extroverted systems) exert greater long-range water structuration than those of globular proteins (introverted systems) differentially impacting their colligative properties.

As a first step we independently tested whether the polymers effectively affect the structure of water. Specifically, we measured the Raman spectra of water in solutions of Gelatin, PEG, IgG and HSA. The results show that the fraction of tetracoordinated water (abundant in ice) increases when the fraction of randomly oriented polymer conformations increases, in the order HSA<IgG<PEG<Gelatin (Figure 4). This is in agreement with previous conclusions reported by Ling and Ochsenfeld[69]. Additionally, these findings are also in line with previous observations obtained using IR methods, showing not only that water rotational dynamics in the protein solutions can be affected in the long-range[72], but also that protein surfaces can produce long range

constraints on water's orientational flexibility[4]. Particularly, this indicates that water is strongly hydrogen bonded and behaves as a coordinated collective in crowded systems[4], in accordance with our observations.

In a second part of our study, we decided to test whether artificial lipid membranes can respond to the structuration of water promoted by introverted and extroverted polymer system. As shown in Figures 2 and 3, water dipolar relaxation of membranes exposed to the different polymer solutions correlates with the Raman results, suggesting a coupling between these two components. Specifically, the extent of water dipolar relaxation in DOPC bilayers decreases following the order Gelatin>PEG>IgG>HSA. This is reflected in the changes observed in all LAURDAN fluorescent parameters, and is evident as a displacement on the L_α-L_β lamellar transition trajectory defined in the phasor plot towards the L_β phase. Interestingly, a similar trend was observed when a native protein was denatured, as shown in Figure 5. In particular, these last results are in harmony with those of Ling and collaborators[69,70], showing that protein denaturation causes a transition from an introverted to an extroverted state, which greatly increases the extent of water structuration. Also, our results with PEG are in concordance with previous observations ascribing dehydration effects on lipid interfaces to long range water structuration promoted by this polymer[37–39], increasing lipid membrane lateral packing and main transition temperature (T_m) when the polymer concentration is increased[38,39,41].

On top of the changes caused by the polymers on the hydration properties of lipid lamellar structures, we want to stress the results observed with membranes composed of DOPC:GMO. As shown in Figure 7, changes in PEG concentration or structural changes caused by denaturation of proteins can induce a transition from a cubic (Pn3m) to a lamellar (L_α) phase in the lipid mixture. It is well known that mesomorphic transitions among different lipid self-assemblies can be isothermally and isobarically induced by changes in hydration[73] (see also Figure S10c in the supporting information). These are produced by the emergence of curvature stress fields, via changes in the membrane lateral pressure profile due to changes in hydration. In particular, the results shown in Figure 7 may be of relevance in biological systems, particularly when the colloidal nature of the cell is considered. This result provides *in vitro* support to our hypothesis, which is that metabolic changes produced in the cell

cytosol (changes in ATP, for example) affect the structure of intracellular proteins which in turn impact water structure and therefore the structure of lipid self-assemblies[20]. A schematic summary of the results and ideas discussed here is provided in Figure 8. It is important to remark, that lipid mesomorphic transitions exerted by these polymers occur at protein/polymer concentrations much higher than those generally used for regular *in vitro* experiments. This observation highlights the importance of working with model systems mimicking the crowded cellular environment when biological membranes are addressed.

Finally, we also want to emphasize the identification and characterization of another type of lipid structural transition using the LAURDAN spectral phasor analysis, specifically the Pn3m→L_α (cubic to lamellar) transition trajectory, which is different to that previously described for the L_α→L_β [32, 68] (both lamellar). In addition this Pn3m→L_α transition trajectory also shows that the linear combination of the two states (i.e., Pn3m and L_α) account for the displacement of the phasor, as shown for the L_β -L_α trajectory (see Figure 1). We also obtained information on physical features of the Pn3m phase of GMO: according to our results, water relaxation is greater in the cubic phase than in the L_α phase (Figure 6). This difference can be interpreted as a consequence of the very curved geometry of this non-lamellar structure [65], which allows faster rotation of water and a larger extent of relaxation near the probe compared with the lamellar structure. In fact, the LAURDAN GP_{ex} value obtained for pure GMO Pn3m phase is in agreement with that observed in micelles composed of complex gangliosides, another type of lipid self-assembly with a highly curve interface[74]. To the best of our knowledge, this is the first time that a full characterization of LAURDAN fluorescence parameters is performed for GMO and its mixtures with DOPC.

5. Concluding remarks and perspectives

Structural coupling between proteins and membranes mediated by changes in water activity as demonstrated in this paper provides an alternative framework to understand cellular processes and information exchange between non-adjacent cellular components[75]. In particular, the colloidal theoretical framework (AIH) considered here may offer alternatives to the prevailing

application of models based on regular solution theory to account for the rapid and coherent responses of cellular physiology. Under this alternative colloidal view cells may exploit an almost instantaneous transfer of information through the intervention of water, acting as a key dynamically and reversibly structured biocomponent [5,20,75]. Furthermore, the fact that lipid mesomorphism can be finely regulated by changes in water activity, which in turn can be governed by metabolic changes on protein structure, may open another way to interpret the role of membranes in biological systems, underlining the integration of lipid mesomorphism as a dynamic phenomenon into the colloidal view of the cell. For example, this can be relevant in the context of the role of coacervation proposed by Rothman in the assembly of highly dynamic organelles such as the Golgi complex [76], whose surface has been generally portrayed as stable lipid bilayers compartmentalizing environments. In fact, cells contain a great percentage of lipids that when isolated, tend to form non-bilayer structures, like micelles, cubic or inverted hexagonal phases [77]. The general relevance of lipid polymorphism in cell biology has been disregarded during the last decades[73,77–80], as well as the key role that water plays in cell function[5,20,75]. As a consequence an integrated view of the cell is still lacking[20,75]. These ideas, which run counter to the generally accepted view of the cell, are critically discussed in great detail in a recent review article published by our group [81], which for the first time offers a possible role for lipid self-assemblies within the framework of the AIH. Specifically, and based on experiments performed in living cells displaying glycolytic oscillations, we concluded that *interfacial* water is coupled (physically linked) to water activity in the cytosol [20]. It “resonates”, as it were, with an oscillating central metabolism. This does not specify what structure the lipids are in, just that it is not static and that it is coupled to metabolism. This “dynamic hydration” can be a controlling factor in the probability of lyotropic mesomorphic transitions, just as protein hydration is intimately related to protein conformational dynamics [82,83], allowing lipid self-assemblies to behave as metabolically reactive structures in the cell.

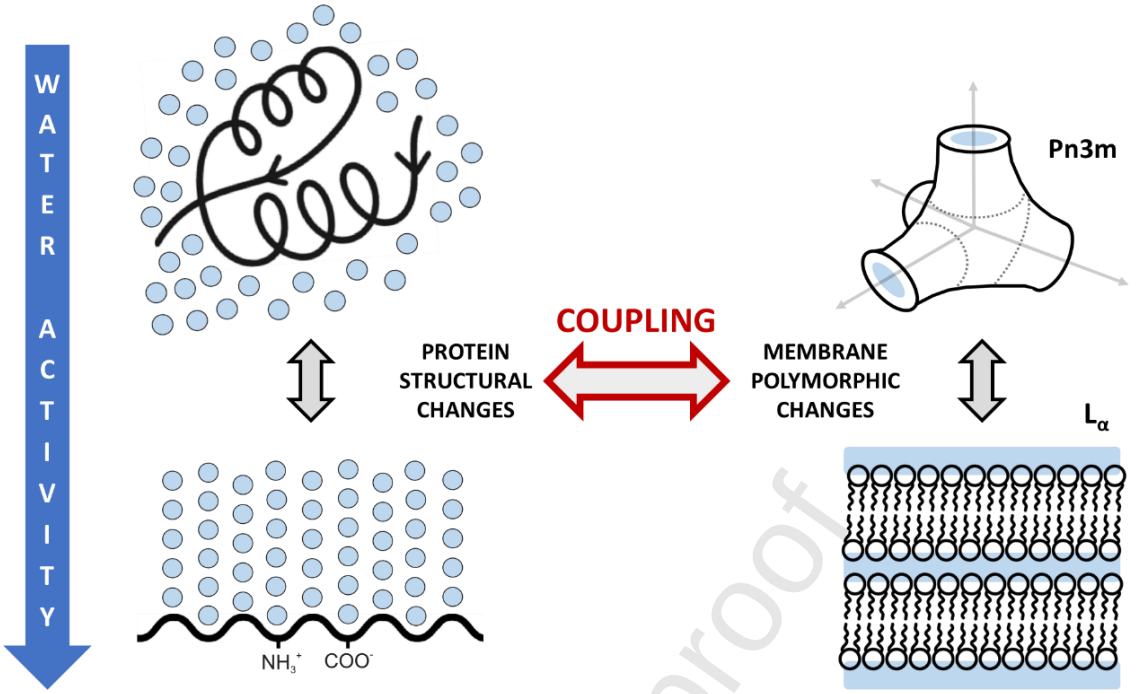

Figure 8. Sketch summarizing the main results obtained in this study. Through changes in protein structure, it is possible to modulate water activity. This effect can be transmitted to membranes, producing changes in hydration and allowing for conversion between different mesomorphic structures. Altogether, this dynamic interplay generates a coupling of protein structure and membrane polymorphism through water activity. Adapted from [20].

Acknowledgements

L.A.B. is a member of the Argentinian Research Council (CONICET) research career, Argentina. A.M is currently a CONICET post-doctoral fellow. We would like to thank to the Dr. Eduardo Coronado and Dr. Gabriela Lacconi (LANN, Argentina) for the technical assistance with Raman experiments, Dr. Macarena Siri for her help with FTIR experiments and data analysis and Dr. Roberto P. Stock for critical reading of the manuscript.

Funding

This work was supported by CONICET and a grant from the Agencia Nacional de Promoción Científica y Tecnológica (PICT, 2017-2658), Argentina.

Author contributions

Agustín Mangiarotti: Conceptualization, Experiments, Figure preparation and analysis, Writing - original draft, Writing - review & editing.

Luis A. Bagatolli: Conceptualization, Writing - original draft, Writing - review & editing, Supervision, Resources and Funding acquisition.

References:

[1] R.J. Ellis, Macromolecular crowding: Obvious but underappreciated, Trends Biochem. Sci. 26 (2001) 597–604. doi:10.1016/S0968-0004(01)01938-7.

[2] S.B. Zimmerman, S.O. Trach, Estimation of macromolecule concentrations and excluded volume effects for the cytoplasm of Escherichia coli, J. Mol. Biol. 222 (1991) 599–620. doi:10.1016/0022-2836(91)90499-V.

[3] P. Ball, Water as a Biomolecule, ChemPhysChem. 9 (2008) 2677–2685. doi:10.1002/cphc.200800515.

[4] J.T. King, E.J. Arthur, C.L. Brooks, K.J. Kubarych, Crowding induced collective hydration of biological macromolecules over extended distances, J. Am. Chem. Soc. 136 (2014) 188–194. doi:10.1021/ja407853c.

[5] M. Chaplin, Do we underestimate the importance of water in cell biology?, Nat. Rev. Mol. Cell Biol. 7 (2006) 861–866. doi:10.1038/nrm2021.

[6] P.M. Kasson, E. Lindahl, V.S. Pande, Water ordering at membrane interfaces controls fusion dynamics, J. Am. Chem. Soc. 133 (2011) 3812–3815. doi:10.1021/ja200310d.

[7] E.A. Disalvo, Membrane hydration: A hint to a new model for biomembranes, Subcell. Biochem. 71 (2015) 1–16. doi:10.1007/978-3-319-19060-0_1.

[8] Y. Shin, C.P. Brangwynne, Liquid phase condensation in cell physiology and disease, Science (80-.). 357 (2017) eaaf4382. doi:10.1126/science.aaf4382.

[9] V.N. Uversky, Intrinsically disordered proteins in overcrowded milieu: Membrane-less organelles, phase separation, and intrinsic disorder, Curr. Opin. Struct. Biol. 44 (2017) 18–30. doi:10.1016/j.sbi.2016.10.015.

[10] L. Jaeken, The neglected functions of intrinsically disordered proteins and the origin of life, Prog. Biophys. Mol. Biol. 126 (2017) 31–46. doi:10.1016/j.pbiomolbio.2017.03.002.

[11] G.N. Ling, A physical theory of the living state: The association-induction hypothesis, Blaisdell Publishing Co.; A Division of Random House Inc., NY, USA, 1962.

[12] G.N. Ling, In Search of the Physical Basis of Life, Springer US, 1984. doi:10.1007/978-1-4613-2667-0.

[13] G.N. Ling, Life at the Cell and Below-Cell Level: The Hidden History of a Fundamental Revolution in Biology, Pacific Press, Nampa, Idaho, 2001.

[14] G.N. Ling, A new theoretical foundation for the polarized-oriented multilayer theory of cell water and for inanimate systems demonstrating long-range dynamic structuring of water molecules, Physiol. Chem. Phys. Med. NMR. 35 (2003) 91–130.

[15] H.S. Thoke, S. Thorsteinsson, R.P. Stock, L.A. Bagatolli, L.F. Olsen, The dynamics of intracellular water constrains glycolytic oscillations in Saccharomyces cerevisiae, Sci. Rep. 7 (2017) 16250. doi:10.1038/s41598-017-16442-x.

[16] H.S. Thoke, L.A. Bagatolli, L.F. Olsen, Effect of macromolecular crowding on the kinetics of glycolytic enzymes and the behaviour of glycolysis in yeast, Integr. Biol. 10 (2018) 587–597. doi:10.1039/c8ib00099a.

[17] H.S. Thoke, L.F. Olsen, L. Duelund, R.P. Stock, T. Heimburg, L.A. Bagatolli, Is a constant low-entropy process at the root of glycolytic oscillations?, J. Biol. Phys. 44 (2018) 419–431. doi:10.1007/s10867-018-9499-2.

[18] L.F. Olsen, R.P. Stock, L.A. Bagatolli, Glycolytic oscillations and intracellular K+ concentration are strongly coupled in the yeast Saccharomyces cerevisiae, Arch. Biochem. Biophys. 681 (2020) 108257. doi:10.1016/j.abb.2020.108257.

[19] H.S. Thoke, A. Tobiesen, J. Brewer, P.L. Hansen, R.P. Stock, L.F. Olsen, L.A. Bagatolli, Tight Coupling of Metabolic Oscillations and Intracellular Water Dynamics in Saccharomyces cerevisiae, PLoS One. 10 (2015) e0117308. https://doi.org/10.1371/journal.pone.0117308.

[20] L.A. Bagatolli, R.P. Stock, L.F. Olsen, Coupled Response of Membrane Hydration with Oscillating Metabolism in Live Cells: An Alternative Way to Modulate Structural Aspects of Biological Membranes?, Biomolecules. 9 (2019) 687. doi:10.3390/biom9110687.

[21] D.M. Jameson, Introduction to Fluorescence, CRC Press, Taylor & Francis Group, Boca Raton, FL, 2014. https://www.routledge.com/Introduction-to-Fluorescence/Jameson/p/book/9780367865702 (accessed February 15, 2021).

[22] R.D. Spencer, G. Weber, Influence of brownian rotations and energy transfer upon the measurements of fluorescence lifetime, J. Chem. Phys. 52 (1970) 1654–1663. doi:10.1063/1.1673201.

[23] J.R. Lakowicz, Principles of fluorescence spectroscopy, Springer, 2006. doi:10.1007/978-0-387-46312-4.

[24] T. Parasassi, G. De Stasio, A. d'Ubaldo, E. Gratton, Phase fluctuation in phospholipid membranes revealed by Laurdan fluorescence, Biophys. J. 57 (1990) 1179–1186. doi:10.1016/S0006-3495(90)82637-0.

[25] T. Parasassi, G. De Stasio, G. Ravagnan, R.M. Rusch, E. Gratton, Quantitation

of lipid phases in phospholipid vesicles by the generalized polarization of Laurdan fluorescence, Biophys. J. 60 (1991) 179–189. doi:10.1016/S0006-3495(91)82041-0.

[26] L.A. Bagatolli, LAURDAN Fluorescence Properties in Membranes: A Journey from the Fluorometer to the Microscope, in: Springer, Berlin, Heidelberg, 2012: pp. 3–35. doi:10.1007/4243_2012_42.

[27] S.S.W. Leung, J. Brewer, L.A. Bagatolli, J.L. Thewalt, Measuring molecular order for lipid membrane phase studies: Linear relationship between Laurdan generalized polarization and deuterium NMR order parameter, Biochim. Biophys. Acta - Biomembr. 1861 (2019) 183053. doi:10.1016/j.bbamem.2019.183053.

[28] T. Parasassi, M. Di Stefano, M. Loiero, G. Ravagnan, E. Gratton, Cholesterol modifies water concentration and dynamics in phospholipid bilayers: a fluorescence study using Laurdan probe, Biophys. J. 66 (1994) 763–768. doi:10.1016/S0006-3495(94)80852-5.

[29] T. Parasassi, A.M. Giusti, M. Raimondi, E. Gratton, Abrupt modifications of phospholipid bilayer properties at critical cholesterol concentrations, Biophys. J. 68 (1995) 1895–1902. doi:10.1016/S0006-3495(95)80367-X.

[30] F. Fereidouni, A.N. Bader, H.C. Gerritsen, Spectral phasor analysis allows rapid and reliable unmixing of fluorescence microscopy spectral images, Opt. Express. 20 (2012) 12729. doi:10.1364/oe.20.012729.

[31] D.M. Jameson, E. Gratton, R.D. Hall, The measurement and analysis of heterogeneous emissions by multifrequency phase and modulation fluorometry, Appl. Spectrosc. Rev. 20 (1984) 55–106. doi:10.1080/05704928408081716.

[32] L. Malacrida, E. Gratton, D.M. Jameson, Model-free methods to study membrane environmental probes: a comparison of the spectral phasor and generalized polarization approaches, Methods Appl. Fluoresc. 3 (2015) 47001. doi:10.1088/2050-6120/3/4/047001.

[33] E. Gratton, M.A. Digman, Laurdan Identifies Different Lipid Membranes in Eukaryotic Cells, in: A. Cambi, D.S. Lidke (Eds.), Cell Membr. Nanodomains, CRC Press, Taylor & Francis Group, Boca Raton, FL, 2014: p. 510. doi:https://doi.org/10.1201/b17634.

[34] N.G. James, J.A. Ross, M. Štefl, D.M. Jameson, Applications of phasor plots to in vitro protein studies, Anal. Biochem. 410 (2011) 70–76. doi:10.1016/j.ab.2010.11.011.

[35] M. Štefl, N.G. James, J.A. Ross, D.M. Jameson, Applications of phasors to in vitro time-resolved fluorescence measurements, Anal. Biochem. 410 (2011) 62–69. doi:10.1016/J.AB.2010.11.010.

[36] O. Golfetto, E. Hinde, E. Gratton, Laurdan fluorescence lifetime discriminates cholesterol content from changes in fluidity in living cell membranes, Biophys. J. 104 (2013) 1238–1247. doi:10.1016/j.bpj.2012.12.057.

[37] B. Maggio, J.A. Lucy, Interactions of water-soluble fusogens with phospholipids in monolayers, FEBS Lett. 94 (1978) 301–304. doi:10.1016/0014-5793(78)80962-4.

[38] K. Arnold, L. Pratsch, K. Gawrisch, Effect of poly(ethylene glycol) on phospholipid hydration and polarity of the external phase, BBA - Biomembr. 728 (1983) 121–128. doi:10.1016/0005-2736(83)90444-3.

[39] K. Arnold, O. Zschoernig, D. Barthel, W. Herold, Exclusion of poly(ethylene glycol) from liposome surfaces, BBA - Biomembr. 1022 (1990) 303–310. doi:10.1016/0005-2736(90)90278-V.

[40] R.I. MacDonald, Membrane Fusion due to Dehydration by Polyethylene Glycol, Dextran, or Sucrose, Biochemistry. 24 (1985) 4058–4066. doi:10.1021/bi00336a039.

[41] S. Sahu, P. Talele, B. Patra, R.S. Verma, A.K. Mishra, A Multiparametric Fluorescence Probe to Understand the Physicochemical Properties of Small Unilamellar Lipid Vesicles in Poly(ethylene glycol)-Water Medium, Langmuir. 36 (2020) 4842–4852. doi:10.1021/acs.langmuir.9b03902.

[42] A. Duconseille, T. Astruc, N. Quintana, F. Meersman, V. Sante-Lhoutellier, Gelatin structure and composition linked to hard capsule dissolution: A review, Food Hydrocoll. 43 (2015) 360–376. doi:https://doi.org/10.1016/j.foodhyd.2014.06.006.

[43] Usoltsev, Sitnikova, Kajava, Uspenskaya, Systematic FTIR Spectroscopy Study of the Secondary Structure Changes in Human Serum Albumin under Various Denaturation Conditions, Biomolecules. 9 (2019) 359. doi:10.3390/biom9080359.

[44] C.E. Giacomelli, M.G.E.G. Bremer, W. Norde, ATR-FTIR study of IgG adsorbed on different silica surfaces, J. Colloid Interface Sci. 220 (1999) 13–23. doi:10.1006/jcis.1999.6479.

[45] V.S. Devi, D.R. Coleman, J. Truntzer, Thermal unfolding curves of high concentration bovine IgG measured by FTIR spectroscopy, Protein J. 30 (2011) 395–403. doi:10.1007/s10930-011-9344-y.

[46] J.H. Muyonga, C.G.B. Cole, K.G. Duodu, Fourier transform infrared (FTIR) spectroscopic study of acid soluble collagen and gelatin from skins and bones of young and adult Nile perch (Lates niloticus), Food Chem. 86 (2004) 325–332. doi:10.1016/j.foodchem.2003.09.038.

[47] A. Duconseille, D. Andueza, F. Picard, V. Santé-Lhoutellier, T. Astruc, Molecular changes in gelatin aging observed by NIR and fluorescence spectroscopy, Food Hydrocoll. 61 (2016) 496–503. doi:10.1016/j.foodhyd.2016.06.007.

[48] P. Díaz-Calderón, L. Caballero, F. Melo, J. Enrione, Molecular configuration of gelatin-water suspensions at low concentration, Food Hydrocoll. 39 (2014) 171–179. doi:10.1016/j.foodhyd.2013.12.019.

[49] R. Galántai, I. Bárdos-Nagy, The interaction of human serum albumin and model membranes, Int. J. Pharm. 195 (2000) 207–218. doi:10.1016/S0378-5173(99)00399-3.

[50] J. Sabín, G. Prieto, J.M. Ruso, P. V. Messina, F.J. Salgado, M. Nogueira, M. Costas, F. Sarmiento, Interactions between DMPC liposomes and the serum blood proteins HSA and IgG, J. Phys. Chem. B. 113 (2009) 1655–1661. doi:10.1021/jp804641e.

[51] G. Weissmann, A. Brand, E.C. Franklin, Interaction of immunoglobulins with liposomes, J. Clin. Invest. 53 (1974) 536–543. doi:10.1172/JCI107587.

[52] C. Choe, J. Lademann, M.E. Darvin, Depth profiles of hydrogen bound water molecule types and their relation to lipid and protein interaction in the human stratum corneum: In vivo, Analyst. 141 (2016) 6329–6337. doi:10.1039/c6an01717g.

[53] C. McKay, N.R. Gomer, S.M. Angel, S.K. Sharma, Remote Raman Spectroscopy for Planetary Exploration: A Review, Appl. Spectrosc. Vol. 66, Issue 2, Pp. 137-150. 66 (2012) 137–150. https://www.osapublishing.org/abstract.cfm?uri=as-66-2-137 (accessed February 15, 2021).

[54] G.N. Ling, A convergence of experimental and theoretical breakthroughs affirms the PM theory of dynamically structured cell water on the theory's 40th birthday, in: Water Cell, Springer Netherlands, 2006: pp. 1–52. doi:10.1007/1-4020-4927-7_1.

[55] G.N. Ling, Experimental Confirmation of the Polarized Multilayer Theory of Cell Water Including Data That Lead to an Improved Definition of Colloids, in: Water Ions Biol. Syst., Springer US, 1985: pp. 79–94. doi:10.1007/978-1-4899-0424-9_9.

[56] H. Qiu, M. Caffrey, The phase diagram of the monoolein/water system: Metastability and equilibrium aspects, Biomaterials. 21 (2000) 223–234. doi:10.1016/S0142-9612(99)00126-X.

[57] J. Briggs, H. Chung, M. Caffrey, The Temperature-Composition Phase Diagram and Mesophase Structure Characterization of the Monoolein/Water System, J.

Phys. II. 6 (1996) 723–751. doi:10.1051/jp2:1996208.

[58] C. V. Kulkarni, W. Wachter, G. Iglesias-Salto, S. Engelskirchen, S. Ahualli, Monoolein: A magic lipid?, Phys. Chem. Chem. Phys. 13 (2011) 3004–3021. doi:10.1039/c0cp01539c.

[59] Z. Karami, M. Hamidi, Cubosomes: Remarkable drug delivery potential, Drug Discov. Today. 21 (2016) 789–801. doi:10.1016/j.drudis.2016.01.004.

[60] A. Ganem-Quintanar, D. Quintanar-Guerrero, P. Buri, Monoolein: A review of the pharmaceutical applications, Drug Dev. Ind. Pharm. 26 (2000) 809–820. doi:10.1081/DDC-100101304.

[61] V. Cherezov, J. Clogston, Y. Misquitta, W. Abdel-Gawad, M. Caffrey, Membrane protein crystallization in meso: Lipid type-tailoring of the cubic phase, Biophys. J. 83 (2002) 3393–3407. doi:10.1016/S0006-3495(02)75339-3.

[62] R.H. Templer, K.H. Madan, N.A. Warrender, J.M. Seddon, Swollen Lyotropic Cubic Phases in Fully Hydrated Mixtures of Monoolein, Dioleoylphosphatidylcholine, and Dioleoylphosphatidylethanolamine, in: Springer, Berlin, Heidelberg, 1992: pp. 262–265. doi:10.1007/978-3-642-84763-9_51.

[63] J.M. Seddon, R.H. Templer, Cubic phases of self-assembled amphiphilic aggregates, Philos. Trans. R. Soc. London. Ser. A Phys. Eng. Sci. 344 (1993) 377–401. doi:10.1098/rsta.1993.0096.

[64] P.O. Eriksson, G. Lindblom, Lipid and water diffusion in bicontinuous cubic phases measured by NMR, Biophys. J. 64 (1993) 129–136. doi:10.1016/S0006-3495(93)81347-X.

[65] K. Das, B. Roy, S. Satpathi, P. Hazra, Impact of Topology on the Characteristics of Water inside Cubic Lyotropic Liquid Crystalline Systems, J. Phys. Chem. B. 123 (2019) 4113–4128. doi:10.1021/acs.jpcb.9b01559.

[66] S. Engström, K. Alfons, M. Rasmusson, H. Ljusberg-Wahren, Solvent-induced sponge (L3) phases in the solvent-monoolein-water system, Prog. Colloid Polym. Sci. 108 (1998) 93–98. doi:10.1007/bfb0117965.

[67] A. Ridell, K. Ekelund, H. Evertsson, S. Engström, On the water content of the solvent/monoolein/water sponge (L3) phase, Colloids Surfaces A Physicochem. Eng. Asp. 228 (2003) 17–24. doi:10.1016/S0927-7757(03)00299-1.

[68] L. Malacrida, S. Astrada, A. Briva, M. Bollati-Fogolín, E. Gratton, L.A. Bagatolli, Spectral phasor analysis of LAURDAN fluorescence in live A549 lung cells to study the hydration and time evolution of intracellular lamellar body-like structures, Biochim. Biophys. Acta - Biomembr. 1858 (2016) 2625–2635. doi:10.1016/j.bbamem.2016.07.017.

[69] G.N. Ling, M.M. Ochsenfeld, Studies on the physical state of water in living cells and model systems. VI., Physiol. Chem. Phys. Med. NMR. 19 (1987).

[70] G.N. Ling, W. Hu, Studies on the physical state of water in living cells and model systems. X., Physiol. Chem. Phys. Med. NMR. 20 (1988).

[71] G.N. Ling, M.M. Ochsenfeld, The physical state of water in living cells and model systems. XII., Physiol. Chem. Phys. Med. NMR. 21 (1989).

[72] S. Le Caër, G. Klein, D. Ortiz, M. Lima, S. Devineau, S. Pin, J.B. Brubach, P. Roy, S. Pommeret, W. Leibl, R. Righini, J.P. Renault, The effect of myoglobin crowding on the dynamics of water: An infrared study, Phys. Chem. Chem. Phys. 16 (2014) 22841–22852. doi:10.1039/c4cp03102d.

[73] J.M. Seddon, Lyotropic Phase Behaviour of Biological Amphiphiles, Berichte Der Bunsengesellschaft Für Phys. Chemie. 100 (1996) 380–393. doi:10.1002/bbpc.19961000324.

[74] L.A. Bagatolli, E. Gratton, G.D. Fidelio, Water dynamics in glycosphingolipid aggregates studied by LAURDAN fluorescence, Biophys. J. 75 (1998) 331–341. doi:10.1016/S0006-3495(98)77517-4.

[75] L.A. Bagatolli, A. Mangiarotti, R.P. Stock, Cellular metabolism and colloids: Realistically linking physiology and biological physical chemistry, Prog. Biophys. Mol. Biol. (2020). doi:10.1016/j.pbiomolbio.2020.06.002.

[76] J.E. Rothman, Jim's View: Is the Golgi stack a phase-separated liquid crystal?, FEBS Lett. 593 (2019) 2701–2705. doi:10.1002/1873-3468.13609.

[77] P.R. Cullis, M.J. Hope, C.P.S. Tilcock, Lipid polymorphism and the roles of lipids in membranes, Chem. Phys. Lipids. 40 (1986) 127–144. doi:10.1016/0009-3084(86)90067-8.

[78] B. de Kruijff, Lipid polymorphism and biomembrane function, Curr. Opin. Chem. Biol. 1 (1997) 564–569. doi:10.1016/s1367-5931(97)80053-1.

[79] M. Rappolt, Chapter 9 The Biologically Relevant Lipid Mesophases as "Seen" by X-Rays, Adv. Planar Lipid Bilayers Liposomes. 5 (2006) 253–283. doi:10.1016/S1554-4516(06)05009-5.

[80] R.M. Epand, Membrane Lipid Polymorphism, in: Humana Press, 2007: pp. 15–26. doi:10.1007/978-1-59745-519-0_2.

[81] L.A. Bagatolli and R.P. Stock. Lipids, membranes, colloids and cells: A long view. BBA - Biomembranes 1863 (2021) 183684. doi: 10.1016/j.bbamem.2021.183684.

[82] P.W. Fenimore, H. Frauenfelder, B.H. McMahon, F.G. Parak, Slaving: solvent fluctuations dynamics and functions, Proc. Natl. Acad. Sci. U. S. A. 99 (2002) 16047–16051.

[83] H. Frauenfelder, P.W. Fenimore, B.H. McMahon, Hydration, slaving and protein function, Biophys. Chem. 98 (2002) 25–48.

Declaration of interests

☒The authors declare that they have no known competing financial interests or personal relationships that could have appeared to influence the work reported in this paper.

☐ The authors declare the following financial interests/personal relationships which may be considered as potential competing interests:

Graphical abstract

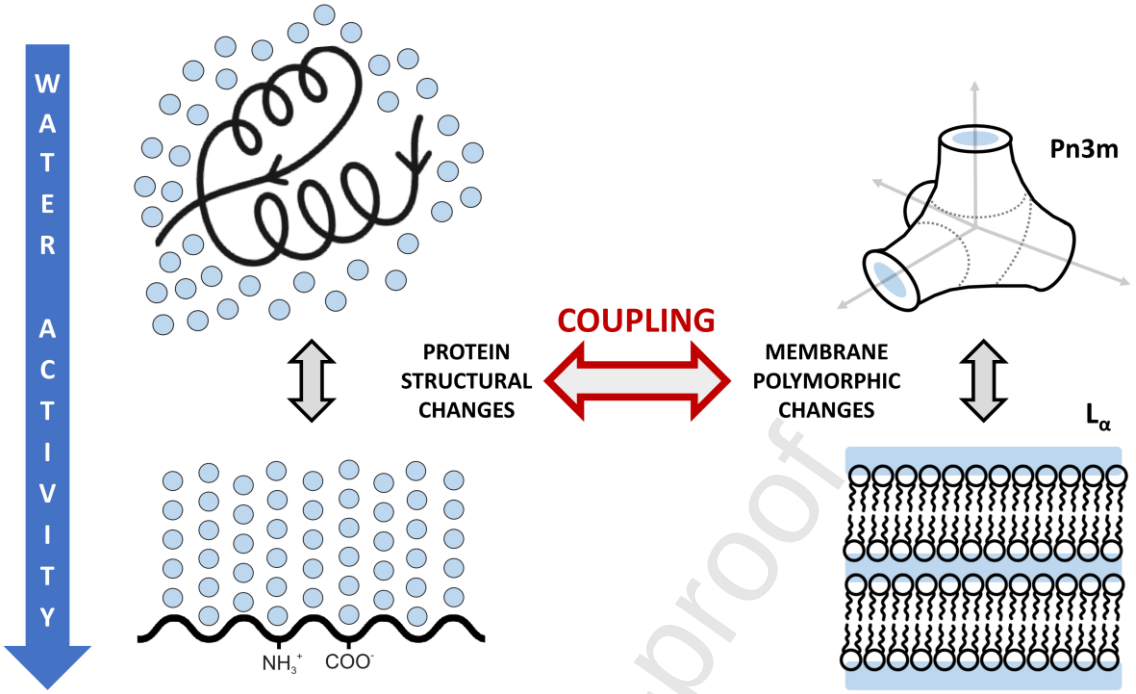

Highlights:

- Macromolecular crowding can modify membrane hydration.
- Distinct protein secondary structures differentially modulate water activity.
- Lipid polymorphism can be induced by proteins existing in extended configurations.

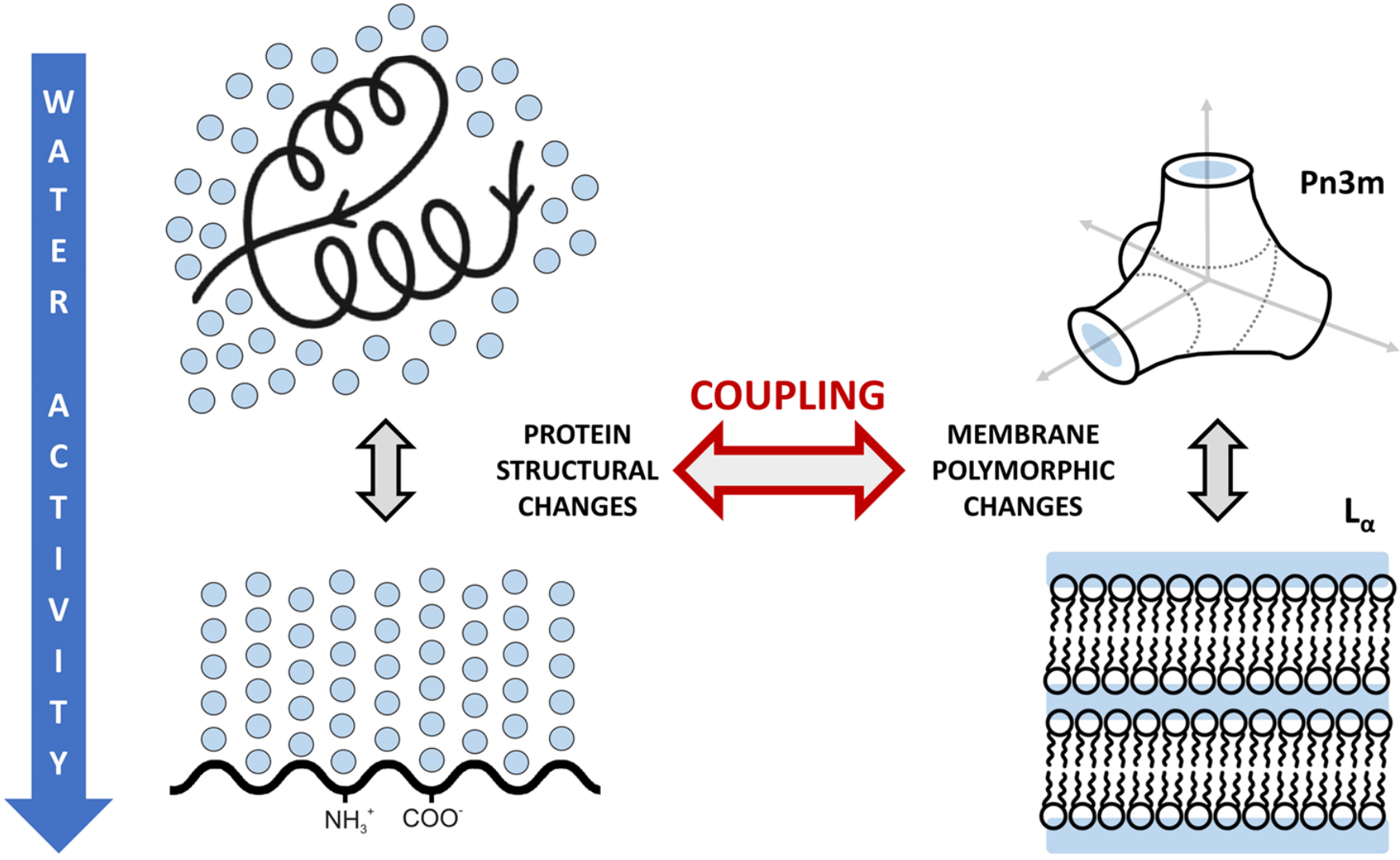

Graphics Abstract

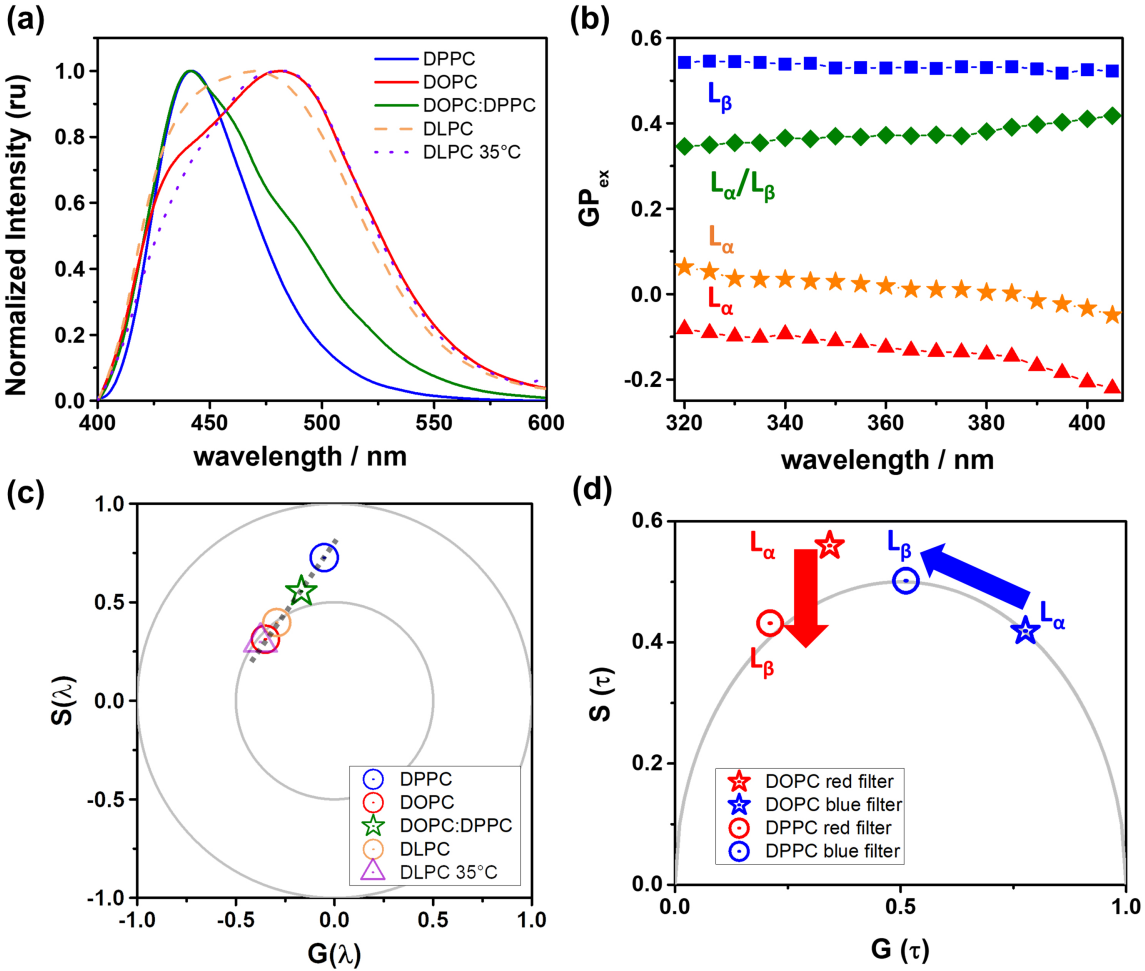
(a)
Normalized Intensity (ru)
wavelength / nm
DPPC
DOPC
DOPC:DPPC
DLPC
DLPC 35°C
(b)
GP$_{ex}$
wavelength / nm
L_β
L_α/L_β
L_α
L_α
(c)
S(λ)
G(λ)
DPPC
DOPC
DOPC:DPPC
DLPC
DLPC 35°C
(d)
S (τ)
G (τ)
L_α
L_β
L_β
L_α
DOPC red filter
DOPC blue filter
DPPC red filter
DPPC blue filter

Figure 1

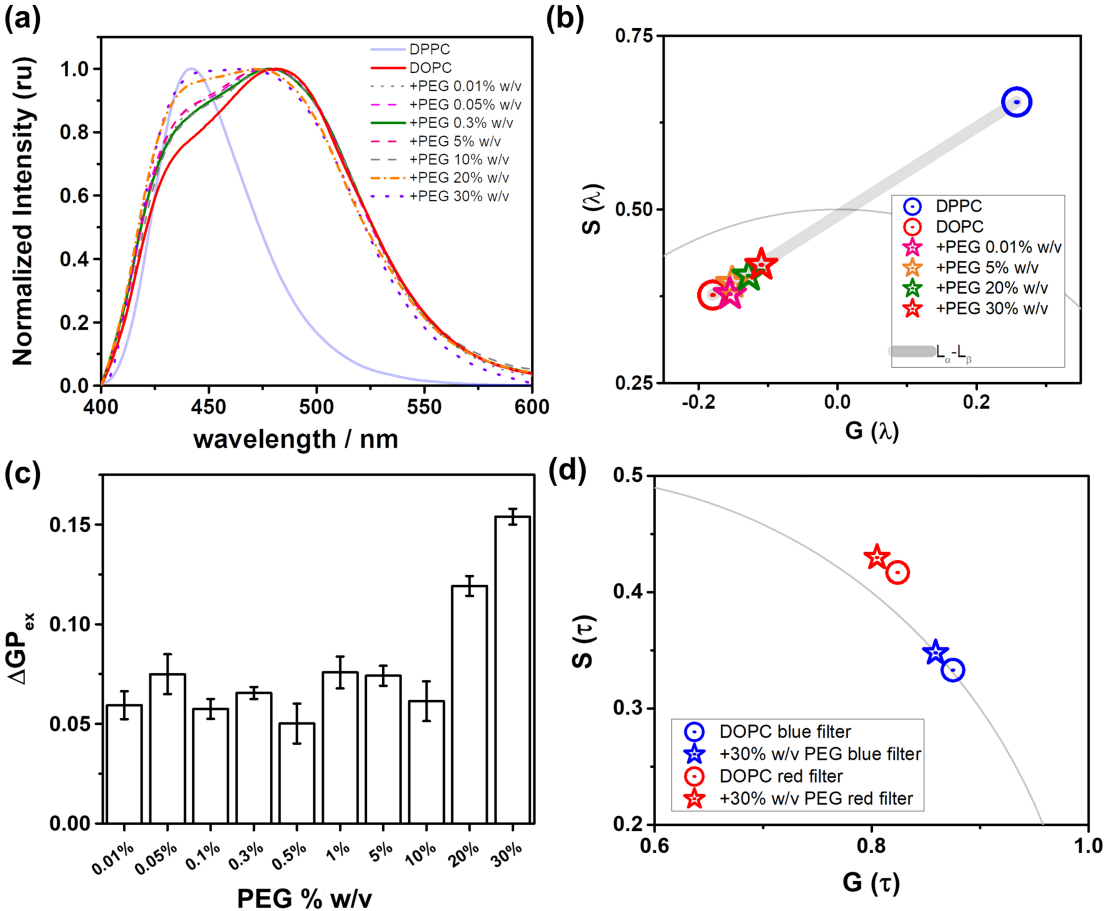
(a)
Normalized Intensity (ru)
wavelength / nm
DPPC
DOPC
+PEG 0.01% w/v
+PEG 0.05% w/v
+PEG 0.3% w/v
+PEG 5% w/v
+PEG 10% w/v
+PEG 20% w/v
+PEG 30% w/v
(b)
S (λ)
G (λ)
DPPC
DOPC
+PEG 0.01% w/v
+PEG 5% w/v
+PEG 20% w/v
+PEG 30% w/v
L$_\alpha$-L$_\beta$
(c)
ΔGP$_{ex}$
PEG % w/v
0.01%
0.05%
0.1%
0.3%
0.5%
1%
5%
10%
20%
30%
(d)
S (τ)
G (τ)
DOPC blue filter
+30% w/v PEG blue filter
DOPC red filter
+30% w/v PEG red filter

Figure 2

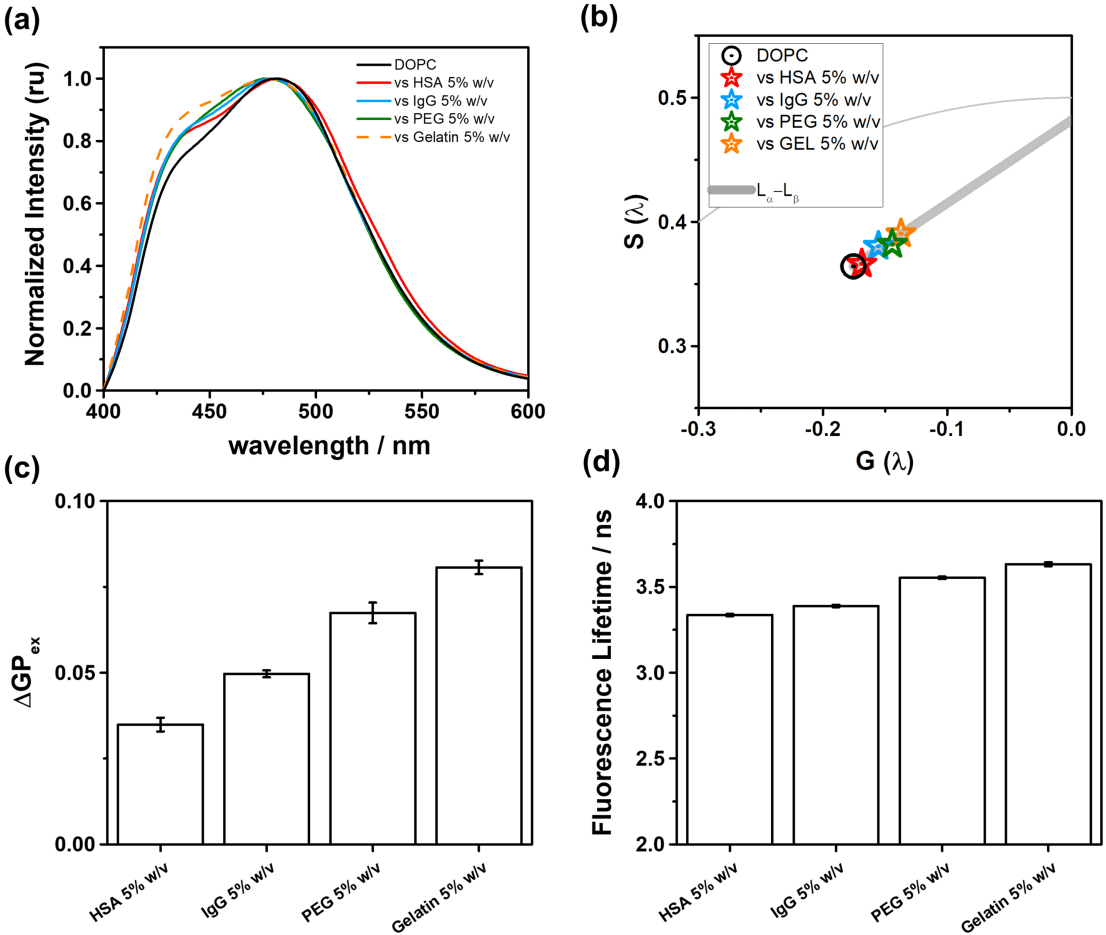
(a)
Normalized Intensity (ru)
wavelength / nm
DOPC
vs HSA 5% w/v
vs IgG 5% w/v
vs PEG 5% w/v
vs Gelatin 5% w/v
(b)
S (λ)
G (λ)
DOPC
vs HSA 5% w/v
vs IgG 5% w/v
vs PEG 5% w/v
vs GEL 5% w/v
Lα–Lβ
(c)
ΔGPex
HSA 5% w/v
IgG 5% w/v
PEG 5% w/v
Gelatin 5% w/v
(d)
Fluorescence Lifetime / ns
HSA 5% w/v
IgG 5% w/v
PEG 5% w/v
Gelatin 5% w/v

Figure 3

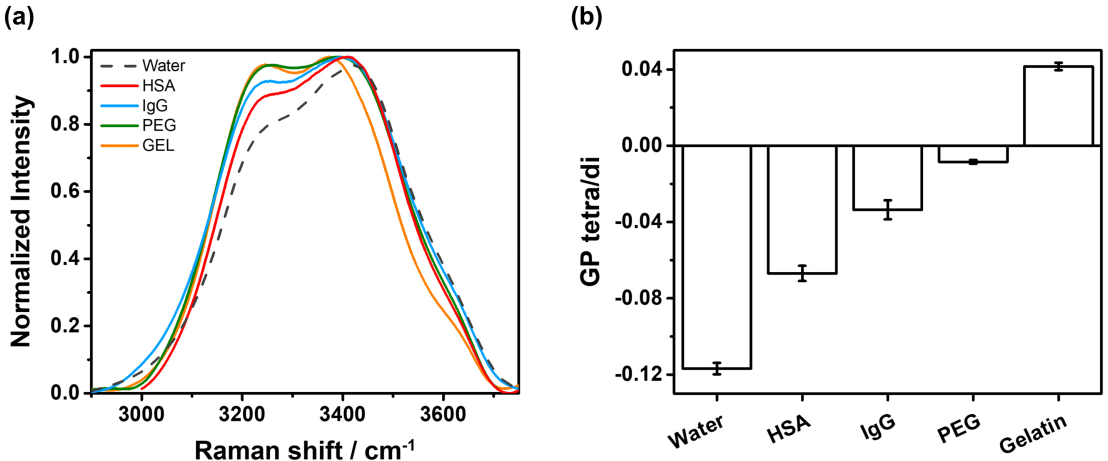
(a)
Water
HSA
IgG
PEG
GEL
Normalized Intensity
1.0
0.8
0.6
0.4
0.2
0.0
3000
3200
3400
3600
Raman shift / cm-1
(b)
GP tetra/di
0.04
0.00
-0.04
-0.08
-0.12
Water
HSA
IgG
PEG
Gelatin

Figure 4

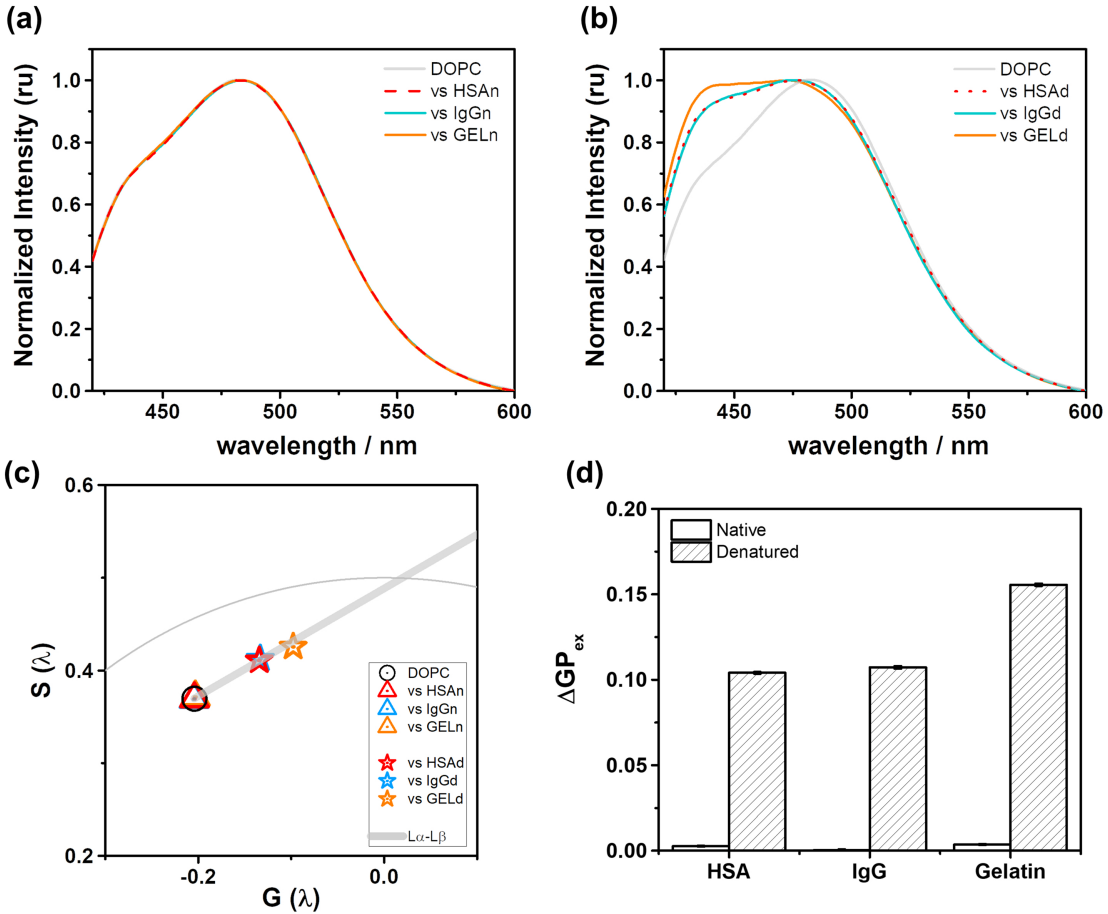
(a)
Normalized Intensity (ru)
wavelength / nm
DOPC
vs HSAn
vs IgGn
vs GELn
(b)
Normalized Intensity (ru)
wavelength / nm
DOPC
vs HSAd
vs IgGd
vs GELd
(c)
S (λ)
G (λ)
DOPC
vs HSAn
vs IgGn
vs GELn
vs HSAd
vs IgGd
vs GELd
Lα-Lβ
(d)
ΔGP ex
Native
Denatured
HSA
IgG
Gelatin

Figure 5

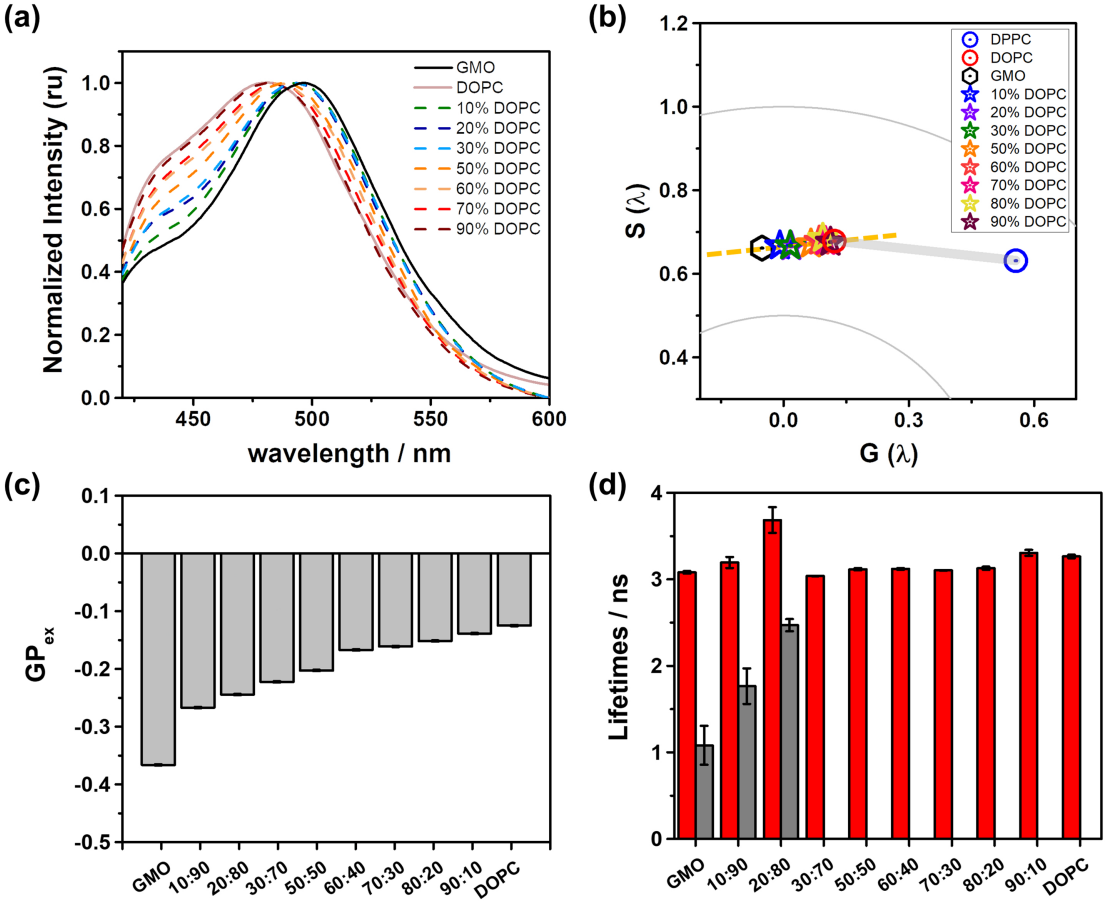
(a)
Normalized Intensity (ru)
wavelength / nm
GMO
DOPC
10% DOPC
20% DOPC
30% DOPC
50% DOPC
60% DOPC
70% DOPC
90% DOPC
(b)
S (λ)
G (λ)
DPPC
DOPC
GMO
10% DOPC
20% DOPC
30% DOPC
50% DOPC
60% DOPC
70% DOPC
80% DOPC
90% DOPC
(c)
GP_ex
GMO
10:90
20:80
30:70
50:50
60:40
70:30
80:20
90:10
DOPC
(d)
Lifetimes / ns
GMO
10:90
20:80
30:70
50:50
60:40
70:30
80:20
90:10
DOPC

Figure 6

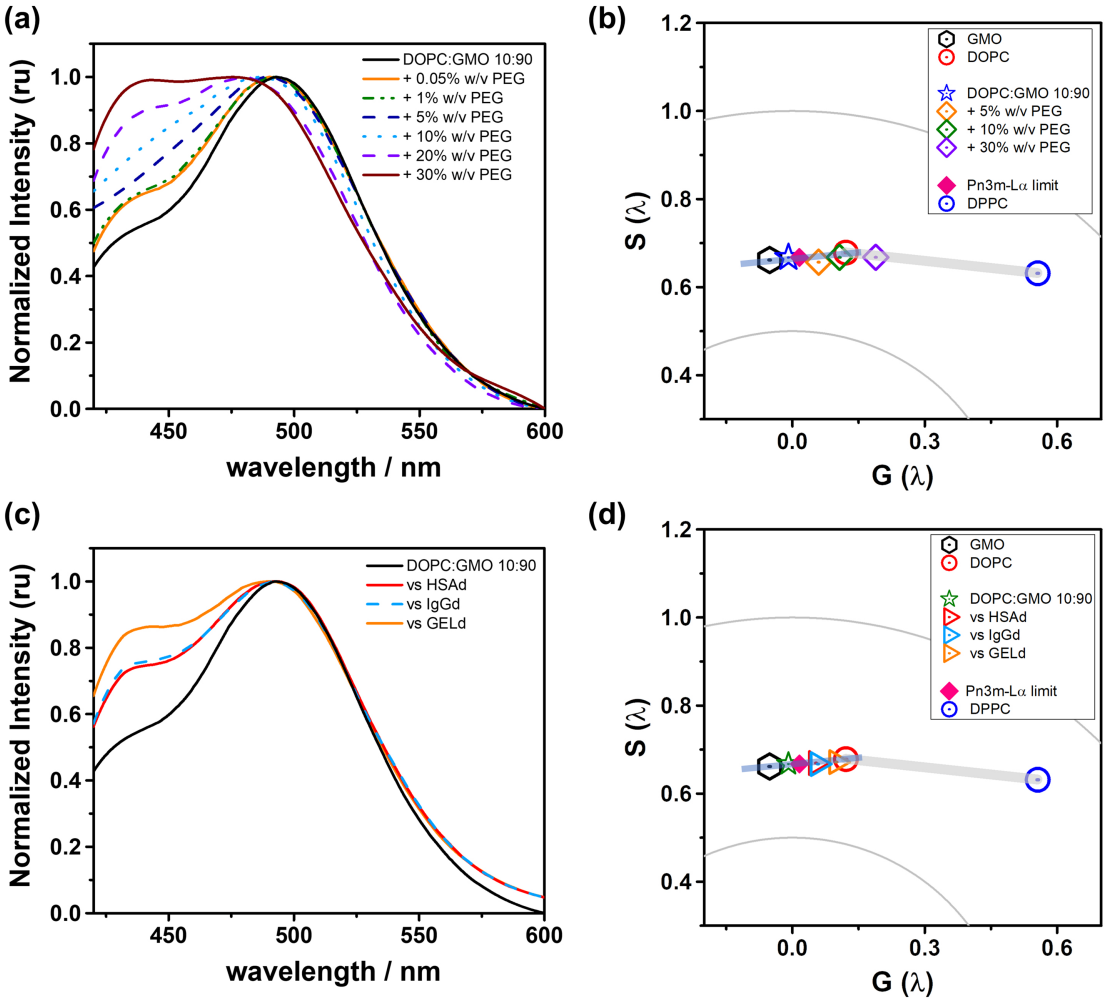
(a)
Normalized Intensity (ru)
wavelength / nm
DOPC:GMO 10:90
+ 0.05% w/v PEG
+ 1% w/v PEG
+ 5% w/v PEG
+ 10% w/v PEG
+ 20% w/v PEG
+ 30% w/v PEG
(b)
S (λ)
G (λ)
GMO
DOPC
DOPC:GMO 10:90
+ 5% w/v PEG
+ 10% w/v PEG
+ 30% w/v PEG
Pn3m-Lα limit
DPPC
(c)
Normalized Intensity (ru)
wavelength / nm
DOPC:GMO 10:90
vs HSAd
vs IgGd
vs GELd
(d)
S (λ)
G (λ)
GMO
DOPC
DOPC:GMO 10:90
vs HSAd
vs IgGd
vs GELd
Pn3m-Lα limit
DPPC

Figure 7

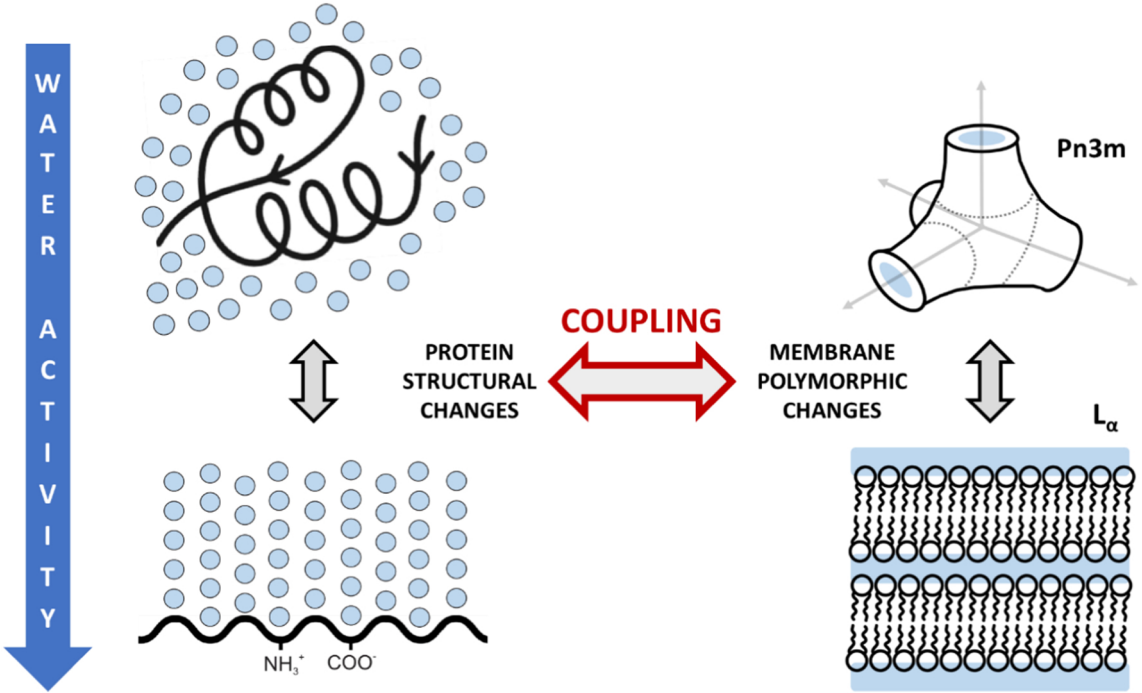
WATER ACTIVITY
COUPLING
PROTEIN STRUCTURAL CHANGES
MEMBRANE POLYMORPHIC CHANGES
Pn3m
L_α
NH_3^+
COO^-

Figure 8